

Chem Soc Rev

Chemical Society Reviews

www.rsc.org/chemsocrev



ISSN 0306-0012



ROYAL SOCIETY
OF CHEMISTRY

REVIEW ARTICLE

Benjamin J. Wiley, Yujie Xiong *et al.*

Oxidative etching for controlled synthesis of metal nanocrystals: atomic addition and subtraction

Oxidative etching for controlled synthesis of metal nanocrystals: atomic addition and subtraction

Cite this: *Chem. Soc. Rev.*, 2014, 43, 6288

Ran Long,^a Shan Zhou,^a Benjamin J. Wiley*^b and Yujie Xiong*^a

Since the discovery of the role of oxidative etching in shape-controlled metal nanostructure synthesis in 2004, it has become a versatile tool to precisely manipulate the nucleation and growth of metal nanocrystals at the atomic level. Subsequent research has shown that oxidative etching can be used to reshape nanocrystals *via* atomic addition and subtraction. This research has attracted extensive attention from the community because of its promising practical applications and theoretical value, and as a result, tremendous efforts from numerous research groups have been made to expand and apply this method to their own research. In this review, we first outline the merits of oxidative etching for the controlled synthesis of metal nanocrystals. We then summarize recent progress in the use of oxidative etching to control the morphology of a nanostructure during and after its synthesis, and analyze its specific functions in controlling a variety of nanocrystal parameters. Applications enabled by oxidative etching are also briefly presented to show its practical impact. Finally, we discuss the challenges and opportunities for further development of oxidative etching in nanocrystals synthesis.

Received 22nd April 2014

DOI: 10.1039/c4cs00136b

www.rsc.org/csr

1. Introduction

Metal nanocrystals have demonstrated a range of fascinating electrical, magnetic and optical properties that are distinct from those of bulk materials.^{1–7} Tailoring the size, shape and

structure (*e.g.*, solid or hollow) of metal nanocrystals opens a window to finely tune the physical and chemical properties.^{1,8–10} These nanocrystals, in turn, have found their applications in many emerging fields such as catalysis for organic reactions,^{11–13} fuel cells^{14,15} and pollutant reduction,¹⁶ localized surface plasmon resonance (LSPR) and surface enhanced Raman scattering (SERS) sensing,^{17–20} electronics,^{21–24} and biomedical imaging and therapy.^{25–28} Many of these applications require the use of metal nanocrystals with precisely controlled parameters, such as size, shape, structure, crystallinity, composition and surface chemistry. Thus, researchers have been and continue to develop

^a Hefei National Laboratory for Physical Sciences at the Microscale, Collaborative Innovation Center of Chemistry for Energy Materials, and School of Chemistry and Materials Science, University of Science and Technology of China, Hefei, Anhui 230026, P. R. China. E-mail: yjxiong@ustc.edu.cn; Fax: +86-551-63606657

^b Department of Chemistry, Duke University, 124 Science Drive, Box 90354, Durham, NC 27708, USA. E-mail: benjamin.wiley@duke.edu



Long Ran

Ran Long was born in Anhui, China, in 1987. She received her BS in Chemistry from the University of Science and Technology of China (USTC) in 2009. Since then she has been studying as a PhD candidate under the tutelage of Professor Yujie Xiong at the USTC. Her research interests focus on controlled synthesis and catalytic applications of metal nanocrystals.



Shan Zhou

Shan Zhou was born in Anhui, China, in 1993. He is currently an undergraduate student at the University of Science and Technology of China, and expects to receive his BS in chemistry (Special Class for the Gifted Young) in 2014. He joined Professor Yujie Xiong's research group as a research assistant in 2012. His research interests focus on controlled synthesis and biomedical and catalytic applications of metal nanostructures.

a synthetic methodology for metal nanocrystals that enables reproducible control over their parameters and thus the study of their structure–property relationship in the context of practical applications.

In the past decade, a series of metal nanocrystals with various geometries have been synthesized by adjusting a number of experimental parameters including the metal precursor, solvent, temperature, the catalyst, the capping agent, and the reducing agent.^{1,2,29–45} Each of these parameters can have an impact on the nucleation and growth of metal nanocrystals, providing the means for controlling the crystallinity and surface facets of nanocrystals.^{1,46} Despite the success in precisely tailoring nanocrystal parameters, many questions regarding how to improve reaction reproducibility and product homogeneity remain unanswered. Indeed, these questions have puzzled the research community since shape-controlled synthesis was first developed (*i.e.* late 1990's and early 2000's).¹ Addressing these questions requires a deeper understanding of the fundamentals behind each synthesis.

In a typical synthesis, the formation of metal nanocrystals can be divided into three stages: nucleation from the atoms formed by reduction of metal salts, evolution of nuclei into seeds, and growth of seeds into nanocrystals through a process of atomic addition.¹ Tremendous efforts have been made to manipulate the way the atoms are added to a seed. For example, nanocrystal growth rates can be manipulated by altering the reducing agent, temperature, solvent, and the capping agent. Basically there are two important aspects of the atomic addition process: one is the reduction rate of ions to zerovalent atoms, and the other is the location where atoms are added to seeds. Once atoms are added to specific locations on the formed seeds, they will act as a template to guide further atomic addition. Without a mechanism for reversing atomic addition, metal nanocrystals can continue to grow to form morphologies that are thermodynamically unfavorable.

As a matter of fact, it is by such a kinetically driven growth mechanisms that various kinds of twinned crystals are generated.

In certain cases, the twinned seeds can evolve into useful nanostructures such as Ag and Cu nanowires for electronics. On the other hand, formation of twinned particles can be an obstacle to the synthesis of high yields of single-crystal products. To overcome this problem, Xia, Wiley and Xiong demonstrated in 2004 and 2005 that oxidative etching can selectively remove twinned structures from face-centered cubic (fcc) metal nanocrystals such as Ag and Pd, respectively,^{47,48} providing a new and important approach to tailoring the crystallinity of nanocrystals.

The essence of oxidative etching is oxidation of zerovalent atoms, clusters and seeds to ionic states by oxidative species such as oxygen and Fe(III)/Fe(II) in solution, together with coordination ligands and/or corrosive ions (*e.g.*, chloride). This effect is not only capable of completely dissolving twinned structures, but also can compete with the reduction of metal precursors to alter the nucleation and growth modes.⁴⁹ As a result, it can enable more precise control over the nucleation and growth of metal nanocrystals in solution. This control in turn enables the tuning of the physical parameters of nanocrystals in a single system without significant variations in surface chemistry. This feature is important for investigating size- or shape-dependent properties that are quite sensitive to the chemical environment around the nanocrystals. In fact, oxidative etching is a technique that has been widely used in the semiconductor industry. For instance, etching is a required step for defining metal electrodes in circuits; wet etching can make various geometries in semiconductors such as silicon with isotropic or anisotropic patterns, complementary to the dry-etching technique.⁵⁰ By applying etching to solution-phase synthesis, the research community has discovered more powerful and versatile knobs that can be tuned to fulfil the requirements for controlled synthesis.

Oxidative etching is a common phenomenon in nature. One familiar example is corrosion in steel by air and water. Similarly, oxidative etching is an unavoidable influential factor induced by the impurities in reagents during nanocrystal synthesis. For example, in the polyol process, a method widely used for



Benjamin J. Wiley

Benjamin J. Wiley received his BS in Chemical Engineering from the University of Minnesota in 2003, and his PhD in Chemical Engineering from the University of Washington in Seattle in 2007 (with Professor Younan Xia). He subsequently worked as a post-doctoral fellow with Professor George Whitesides at Harvard University. He started as an Assistant Professor in the Department of Chemistry at Duke University in 2009. His work focuses on the

production, properties, and applications of metal nanostructures. To date he has published 60 papers with over 7000 citations, has 5 patent applications, and received an NSF CAREER award.



Yujie Xiong

Yujie Xiong received his BS in chemical physics in 2000 and PhD in inorganic chemistry in 2004 (with Professor Yi Xie), both from the University of Science and Technology of China (USTC). After four-year training with Professors Younan Xia and John A. Rogers, he joined the NSF-NNIN at Washington University in St. Louis as the Principal Scientist and Lab Manager. Starting from 2011, he is a Professor of Chemistry at the USTC. He has

published 83 papers with over 7000 citations (H-index 45). His research interests include synthesis, fabrication and assembly of inorganic materials for energy and environmental applications.

the synthesis of metal nanocrystals, polyols such as ethylene glycol (EG) serve as solvent and reducing agents. EG contains impurities of chloride and ferric, both of which can corrode metals. The corrosive effect of these impurities can be essentially zero or very significant, depending on the chemical environment. When we examine the history of metal nanocrystal synthesis, we find that these factors were not considered prior to their discovery in 2004.^{32,48,51–57} If the role of etching is not considered, it can often be difficult to obtain reproducible synthetic results. In most cases, it is not feasible to completely eliminate impurities from reaction systems. Since the etching effect cannot be easily avoided, it would be ideal to develop methods to overwrite its influence on the synthesis and/or to harness oxidative etching to make a desired product. When oxidative etching is tightly controlled in the synthesis, it not only can maneuver the physical parameters of nanocrystals, but also give birth to totally new geometries which exhibit fascinating properties.

In addition to parameter control, preserving the geometry of nanocrystals represents another grand challenge to nanoscience. For instance, extensive studies have shown that the shape of a metal nanocrystal can undergo dynamic (and sometimes reversible) changes in response to variations in the surrounding environment. Among various environmental factors, oxidative etching has been shown to cause morphological changes.^{32,48,51–57} Despite this negative role of oxidative etching, it potentially provides an ingenious and facile way to access new nanocrystal shapes if controlled appropriately. In contrast to the growth of nanocrystals (*i.e.*, addition of atoms), oxidative etching is essentially subtraction of atoms from existing nanocrystals. With a deep understanding of oxidative etching, one can intuitively employ it to carve metal nanocrystals into desired shapes.

From the overview above, we introduce the reader to the role of oxidative etching in controlled synthesis. First, it offers precise control over the nucleation and growth of metal nanocrystals at the atomic level, and enables direct manipulation of the populations of atoms, clusters and nanocrystals during their synthesis (see Fig. 1). Second, the nanocrystals size or shape can be tightly controlled while other parameters such as surface chemistry are changed to a minimal extent, enabling the investigation of the size- or shape-dependent plasmonic and catalytic properties free of the influence from the other factors. Third, it provides for the possibility of reshaping the nanocrystals *via* atomic addition/subtraction and refining their functions for specific applications.

Overall, as a complement to atomic addition, oxidative etching has become a highly important process in the field of metal nanocrystals synthesis. As the chemical and physical properties of metal nanocrystals have a strong correlation with their morphologies, tuning the parameters of metal nanocrystals by oxidative etching will undoubtedly expand their utilization in various research fields. As such, this topic significantly impacts researchers not only in chemistry, but also in physics, materials science, optics, chemical engineering, and electrical engineering. Thus this review article aims to summarize and analyze its fundamentals and recent developments which will in turn hopefully facilitate its further application.

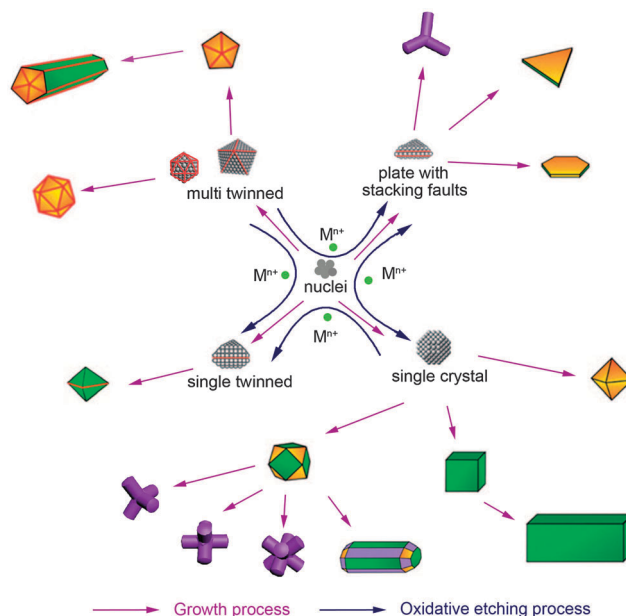


Fig. 1 Summary of reaction pathways affected by oxidative etching, leading to fcc metal nanocrystals with different shapes.

In this review article, we focus on the recently developed strategies for the synthesis of metal nanocrystals that used oxidative etching, and highlight the common mechanisms in various synthetic systems and approaches. Given that metal elements account for 2/3 of the periodic table, we will narrow our discussion down to the system of fcc metals. In the first part of this review, we describe the nature of oxidative etching in order to understand its effect on the synthesis of nanoscale metal materials. We then discuss a series of important control factors enabled by oxidative etching. We finish the synthetic discussion by showing how oxidative etching can be employed as a post-synthesis tool for atomic addition and subtraction to maneuver the size, structure and shape of metal nanocrystals. In the last section of this review, we highlight a few applications enabled by catalytic and optical properties tuned with oxidative etching.

2. Oxidation etching for controlled synthesis and nanocrystal evolution

As mentioned above, three stages are involved in a typical process of direct nanocrystals synthesis: (1) nucleation from the reduction of metal ions, (2) evolution from nuclei into seeds, and (3) growth of seeds into nanocrystals.¹ Oxidative etching plays a central role at each stage and in certain cases can have complex and interlinked effects on all the stages. For instance, the etching can have multiple functions – control of single-crystal *versus* twinned structures, manipulation of the rates of atomic addition, and surface activation to provide sites for atomic addition, all of which may be operative in a single synthesis (refer to the synthesis of Pt multipods in Section 2.1.3.3). In the first part of this section, we will discuss the roles of oxidative etching in

controlling the structure, size and shape of metal nanocrystals, from the viewpoint of nucleation and growth mechanisms. Second, we will analyze the impact of oxidative etching on the evolution of existing nanocrystals through atomic addition and subtraction in a post-synthesis process. Finally, a list of common etchants and their selection rules are summarized to facilitate the future development of oxidative etching techniques.

2.1 Oxidative etching in nucleation and growth stages

Nucleation and growth together with reduction of metal precursors (*i.e.*, atomic supply) comprise the synthesis of metal nanocrystals. As illustrated in Fig. 1, the geometry of a nanocrystal is mainly determined by two key factors: the structure of seeds (single-crystal *versus* twinned) formed in the nucleation and nuclei evolution stages to define a group of shapes, and the surface facets selected in the growth stage for obtaining one specific shape. The formation of seeds (including the nucleation and evolution from nuclei to seeds) is the cornerstone of subsequent growth, and as such, the control of crystallinity will be discussed first. In the nucleation stage, particle size – another physical parameter key to the properties and applications of metal nanocrystals – can also be tuned, which will be demonstrated using specific examples. We will also highlight how kinetic control and anisotropic growth may drive the growth of nanocrystals into non-symmetric modes. Oxidative etching can make important contributions to all of these processes.

The major motivation to utilize oxidative etching is that subtle changes in the reaction conditions can have a dramatic impact on the experimental results. In particular, to develop cost-effective syntheses, it is preferable that synthesis is conducted in air at low temperatures, and avoids the use of expensive ultra-pure chemicals/solvents. In this case, O₂ and other impurities such as chloride and ferric ions are present in the reaction throughout the entire synthesis process, which significantly influence the nucleation and growth through etching. The concentrations of impurity ions in solvents and chemicals vary depending on the batch and manufacturer. Introducing additional etchants at given concentrations into the system is a convenient and controllable solution to avoid synthesis irreproducibility caused by variations in the starting concentration of contaminants.

2.1.1 Structure control (single-crystal *versus* twinned). The structure of seeds determines the crystallinity of the nanocrystals (single-crystal *versus* twinned) obtained from the growth stage. For instance, five-fold twinned, single-twinned and single-crystal seeds can evolve into three different categories of nanocrystal geometries, respectively: (1) multiply twinned nanorods and nanowires, decahedra, and icosahedra; (2) single-twinned right bipyramids and nanobeams; (3) single-crystal cubes, octahedra, tetrahedra, and their various truncated derivatives.

2.1.1.1 Ag. Ag nanostructures have widespread applications in SERS,^{17–19,58} catalysis and electronics.^{22–24,59} Silver was the first case, demonstrated by Wiley and Xia, for which it was shown that oxidative etching could dissolve five-fold twinned structures of a fcc metal.⁶⁰ The five-fold twinned seeds

generally have a decahedral structure. A decahedron can be considered as the assembly of five single-crystal tetrahedral units in which each tetrahedron has two sides in contact with its neighbor through the {111} twin plane. However, this structure does not completely fill space, and thus causes lattice distortion and internal strain.² A similar situation occurs for icosahedra having even more twin boundary defects inside. Due to these defects, the multiply twinned seeds are more susceptible to an oxidative environment than single crystals, and can be selectively removed by oxidative etching.⁶⁰

As compared with other fcc metals, the size window that favors Ag five-fold twinned structures is much broader,⁶¹ making twinned particles more abundant under most reaction conditions.^{60,62} As a result, the removal of twinned seeds by the oxidation etching appears to be vital to the case of Ag. To enhance the strength of oxidative etching, extra chloride ions are typically introduced into the reaction system. Xia *et al.* successfully prepared Ag nanocrystals with a variety of geometries (including nanocubes, cuboctahedra, and nanowires) in the polar solvent ethylene glycol (*i.e.*, the so-called “polyol process”), by employing oxidative etching with Cl[−]/O₂ etchants.^{60,62} At an early stage, both twinned and single-crystal seeds are generated in the synthesis (Fig. 2a). As the reaction proceeds, the twinned seeds are selectively dissolved by etching with O₂ and HCl or NaCl (Fig. 2c), eventually leaving the single-crystal nanocubes behind (Fig. 2d and e). This finding provided a new approach to making high-purity single-crystal nanocrystals. When oxidative etching is blocked by eliminating O₂ from the reaction system, twinned decahedral seeds can grow into nanowires (Fig. 2b). As such, the structure of Ag seeds can be rationally tailored by tuning the knob of oxidative etching. This advance has enabled the synthesis of Ag nanocrystals with controllable crystallinity at high yields, providing a platform for tuning size (see Section 2.1.2).^{65–67} Given that chloride is an inevitable impurity in ethylene glycol, the use of oxidative etching not only offers controllability over the product crystallinity but significantly improves the synthesis reproducibility.

In addition to halogen ions, iron species are another common impurity in polar solvent. In the polyol process, Fe(III) species are reduced by the ethylene glycol to Fe(II), which can react with the oxygen adsorbed on the metal surface and potentially the oxygen dissolved in the solvent. As a result, no matter whether ferric or ferrous ions are added to the system, twinned nanowires are produced (Fig. 2f and i), as long as the added amounts of iron species are sufficient to remove the oxygen and eliminate the etching effect.⁶³ However, when the concentrations of iron species are low, the synthesis mainly yields single-crystal nanocubes (Fig. 2g) as oxidative etching by the remaining oxygen can selectively remove twinned seeds. Apparently, this unique system constitutes a competition between the reduction by ethylene glycol and the oxidation by oxygen on the surface of metal nanoparticles, establishing equilibrium between different valences of iron species. Similarly to the iron species, the Cu(II)/Cu(I) pair has the capability to consume oxygen so that it can control the strength of oxidative etching to yield various structures, such as single-crystal cubes (Fig. 2j), octahedra and their

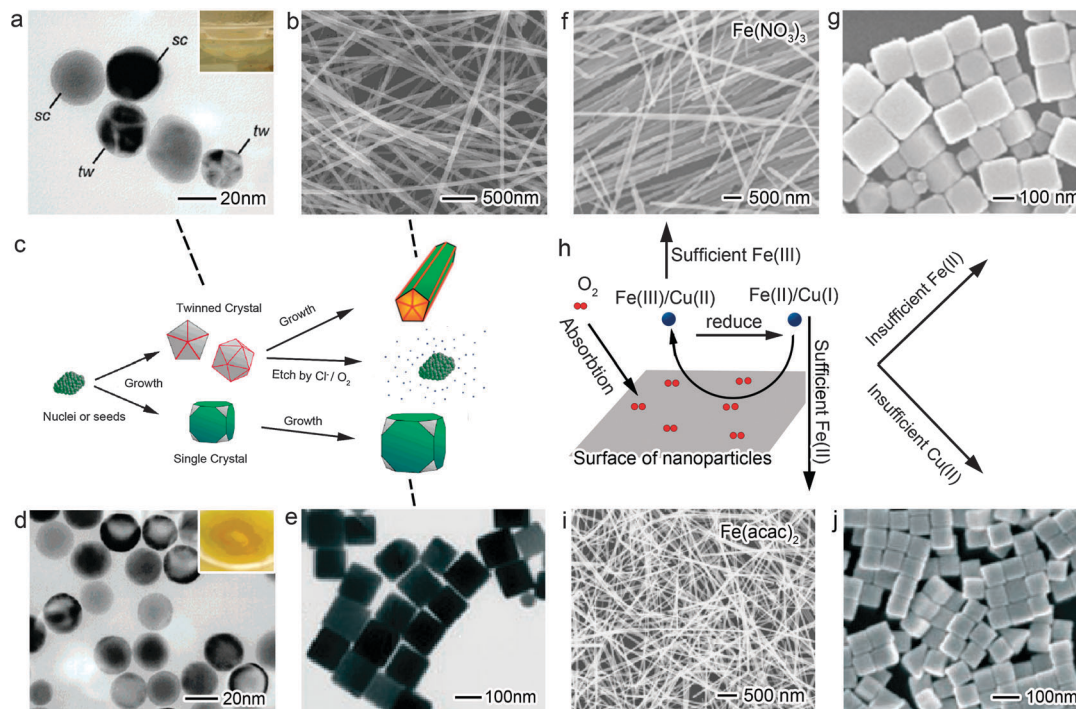


Fig. 2 (a–e) TEM/SEM images of Ag nanocrystals synthesized in EG in the presence of chloride and the corresponding schematic illustrating the role of Cl^-/O_2 : (a) mixture of twinned and single-crystal structures obtained at 2 h, in the presence of NaCl in air; (b) twinned nanowires obtained at 90 min, with trace NaCl but in the absence of oxygen; (c) schematic illustration of oxidative etching *versus* growth with Cl^-/O_2 etchants; (d) single-crystal products obtained at 44 h 10 min, in the presence of trace NaCl in air (adapted with permission from ref. 60, Copyright 2004 American Chemical Society); (e) single-crystal nanocubes obtained with trace HCl in air (adapted with permission from ref. 62, Copyright 2005 Wiley-VCH Verlag GmbH & Co.). (f–j) TEM/SEM images of Ag nanocrystals synthesized with iron species and corresponding schematic illustrating the role of $\text{Fe(III)}/\text{Fe(II)}$: (f) nanowires obtained with sufficient $\text{Fe}(\text{NO}_3)_3$; (g) nanocubes prepared with insufficient $\text{Fe}(\text{acac})_2$ (adapted with permission from ref. 63, Copyright 2005 American Chemical Society); (h) schematic illustration that Fe(II) removes oxygen from the surface of Ag nanoparticles; (i) nanowires prepared with sufficient $\text{Fe}(\text{acac})_2$ (adapted with permission from ref. 63, Copyright 2005 American Chemical Society); (j) nanocubes prepared with CuCl_2 (adapted with permission from ref. 64, Copyright 2006 Wiley-VCH Verlag GmbH & Co.).

intermediate geometries, or twinned nanowires,^{64,68} depending on the concentrations of copper species. In general, high concentrations of cations can ensure that the reaction system is free of oxidative etching, while insufficient amounts are unable to prevent the etching and in some cases may promote it.

In discussing halogen etchants, it is necessary to highlight the function of bromide particularly in the case of Ag. Bromide ions have a relatively weak etching ability compared to chloride, but exhibit an impressive effect on the synthesis of Ag nanocrystals given that Ag is relatively active among the fcc metals and AgBr has very low solubility (see Table 1). It has been demonstrated that oxidative etching by Br^-/O_2 is such that five-fold twinned seeds with high internal strain are removed but single-twinned structures can remain to grow into right bipyramids (Fig. 3a).⁶⁹ To make the etching work better, bromide

should be added prior to the presence of the Ag precursor; otherwise, the presence of five-fold twinned structures cannot be completely prevented (Fig. 3b). It is worth pointing out that the solubility of all the silver halides is very limited, so the concentrations of halogen etchants should be kept extremely low to avoid the precipitation of silver halides.

Oxidative etching can work in an organic medium as well, enabling high-yield production of single-crystal nanocrystals.³⁰ Analogous to the ethylene glycol and aqueous systems, multiply twinned structures dominate the products when oxidative etching is blocked by the replacement of air with argon (Fig. 3c). If the reaction system is switched to air, the population of twinned structures decreases (Fig. 3d), showing the role of oxidative etching in removing twinned seeds. The etching can be further enhanced by ferric species, leading to the formation of single-crystal nanocubes with yields approaching 100% (Fig. 3e and f). Apparently, here the ferric species plays a quite different role from the EG system, mainly because the reduction of Fe(III) to Fe(II) does not occur in the absence of an appropriate reducing agent. The oleylamine used in this system contains a $\text{C}=\text{C}$ and an amine group; the reducing ability of these groups is much less than the hydroxyl and aldehyde groups of EG and its derivatives.^{71,72} As a result, the Fe(III) ions are not reduced but instead can

Table 1 Standard solubility product constants involved in oxidative etching⁷⁰

	K_{sp}
AgCl	1.77×10^{-10}
AgBr	5.35×10^{-13}
AgI	8.52×10^{-17}

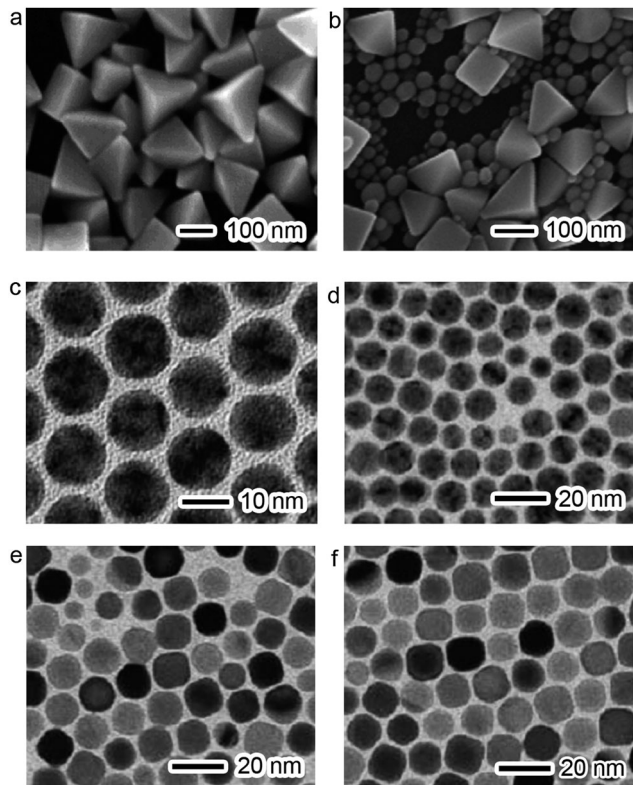


Fig. 3 SEM images of Ag nanocrystals prepared in EG in the presence (a) and absence (b) of NaBr, respectively (adapted with permission from ref. 69, Copyright 2006 American Chemical Society). TEM images of Ag nanocrystals prepared in oleylamine: (c) under argon protection; (d) in air; (e) in air and in the presence of $\text{Fe}(\text{acac})_3$; (f) in air and in the presence of FeCl_3 (adapted with permission from ref. 30, Copyright 2010 Royal Society of Chemistry).

oxidize zerovalent Ag (refer to the standard potentials of ferric and silver ions), facilitating the dissolution of twinned seeds. It is worth pointing out that the standard potential only serves as a reference value since it may be influenced by many other factors such as pH and ligand complexation.

Overall, the synthesis of Ag multiply twinned *versus* single-crystal structures can be manipulated by employing or blocking oxidative etching during the reactions. A few experimental parameters, including inert gas protection and addition of cations and halogen species, have been identified as useful knobs for tuning the strength of etching. The improved control over product homogeneity enabled by the etching has boosted the applications of Ag nanostructures in the past 10 years.

2.1.1.2 Pd. Pd is an excellent catalyst in various applications such as organic synthesis (including coupling reactions,⁷³ hydrogenation reactions⁷⁴ and oxidation reactions⁷⁵), fuel cells,⁷⁶ and pollutant reduction.¹⁶ When the size of Pd materials enters the nanoscale regime, the catalytic activity and selectivity are highly dependent on their physical parameters. As such, controlled synthesis holds the promise for tuning their catalytic performance.

In 2005, Xiong and Xia revealed that Cl^- and O_2 can dissolve Pd nanoparticles through oxidative etching.⁴⁸ Similar to the

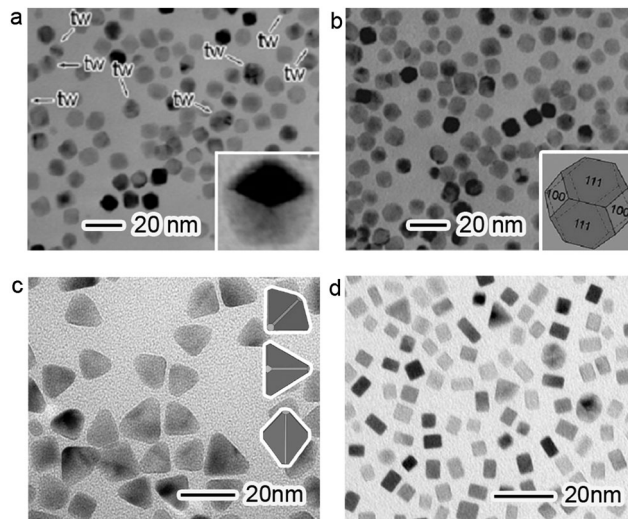


Fig. 4 TEM images of Pd nanoparticles prepared in EG in air at $t =$ (a) 5 min and (b) 3 h, respectively (adapted with permission from ref. 48, Copyright 2005 American Chemical Society). TEM images of Pd nanocrystals prepared in EG in the presence of (c) NaI and (d) NaBr, respectively (adapted with permission from ref. 55, Copyright 2013 American Chemical Society).

case of Ag, twinned Pd structures are more susceptible to the oxidative etching effect relative to their single-crystal counterparts. As the frequently used Pd precursors Na_2PdCl_4 and K_2PdCl_4 contain significant amounts of chloride, the selective removal of twinned seeds by the Cl^-/O_2 etching can be easily implemented in any Pd synthesis in air. As shown in Fig. 4a, a sample from the early stage of the reaction contains 90% single-crystal nanoparticles and 10% twinned structures. In comparison with the Ag system, the portion of twinned structures is lower, potentially due to the narrow size window that favors Pd decahedra and icosahedra.⁷⁷ As the reaction proceeds, the twinned nanoparticles gradually dissolve, leaving high-purity single crystals in the product (Fig. 4b). This finding in 2005 constitutes a platform for controlled synthesis of Pd nanostructures, which made it possible to obtain many different novel geometries in the Pd system in the following years.⁴⁶ In fact, the etching function of O_2 together with halogen ions can better work in the Pd system, as the formation of complex species $[\text{PdX}_4]^{2-}$ facilitates the oxidation of zerovalent Pd. The addition of halogen ions at high concentrations does not produce precipitates analogous to AgCl and AgBr in the case of Ag, so that the concentration range over which one can use halide etchants for the synthesis of Pd single crystals is less restrictive.

Alternatively, one has to block oxidative etching when designing a synthesis for twinned structures in high yields. The Pd surface has relatively strong binding to oxygen so it is not feasible to completely eliminate an oxidative environment from reaction systems by flowing an inert gas through the reaction solution. Thus far a few different approaches have been developed to address this challenge. For example, citric acid has been recognized as an agent that can remove oxygen from Pd surfaces and prevent oxidative etching.⁷⁷ As a result,

the implementation of citric acid into the Pd synthesis enables the production of five-fold twinned icosahedra with high purity.

In addition to chloride, bromide and iodide ions can play more sophisticated roles in the controlled synthesis of Pd nanocrystals. It has been demonstrated that these two halides can promote the formation of Pd{100} surface facets.³² Cubooctahedra are generally the predominant single-crystal Pd products in the absence of capping agents, as this nearly spherical shape has a minimal surface area and is thus thermodynamically favorable.¹ As shown in Fig. 4c and d, the shapes of Pd nanocrystals have been tuned to those enclosed by {100} facets when iodide and bromide are introduced into the synthesis.⁵⁵ The only difference between the two cases lies in the crystallinity of final products caused by the different etching strength of iodide and bromide. Iodide is not as corrosive as the bromide, and as a result, the single-twinned seeds can be maintained to grow into right bipyramids (Fig. 4c). The dual functions of bromide as an etchant and a promoter of {100} facets facilitate the formation of well-defined Pd nanocubes, providing a robust synthetic system for size-controlled synthesis (discussed in the next section).^{16,32} This synthetic protocol is also the most popular one for the production of uniform Pd nanocrystals for catalytic applications.^{16,55,75}

2.1.1.3 Au. Au nanocrystals do not corrode under most conditions, and have large optical cross sections, making them attractive for a wide variety of applications in chemical and biological sensing.^{1,28,78–80} As Au also has excellent biocompatibility, the scattering and absorption (*i.e.*, photothermal effect) from Au nanostructures can be used for imaging and therapy, respectively, in biomedicine.^{28,79} The LSPR band position, intensity and ratio of scattering to absorption have a strong correlation with the physical parameters of Au nanocrystals, and thus control over nucleation and growth holds the key to the further development of their applications.

Similar to the case of Ag, the Cl⁻/O₂ pair is a powerful etchant for both the nuclei and seeds in the Au system.^{81,82,84} As Au is a metal with relatively low reactivity, it requires higher concentrations of chloride to induce oxidative etching compared to Ag. When a small amount of chloride is used, the etching effect is weak, and the products contain a mixture of single-crystal, single-twinned and multi-twinned nanocrystals (Fig. 5a).⁸¹ As the chloride concentration increases, the strength of oxidative etching can be enhanced to completely remove the twinned structures (Fig. 5b). It is worth emphasizing that oxidative etching is a joint effect caused by the oxygen and chloride in all cases. The oxidation is carried out by oxygen, while the chloride mainly enhances the corrosive process. For this reason, the formation of twinned structures cannot be prevented when the reaction is performed in an inert gas environment (Fig. 5c). Alternatively, introducing more oxygen into the system promotes oxidative etching, and the twinned structures can be completely dissolved by fully exposing the reaction to oxygen even when the concentration of chloride is not very high (Fig. 5d).

In the course of etching, surface chemistry also plays a vital role. In the case that the surface is tightly protected by a passive

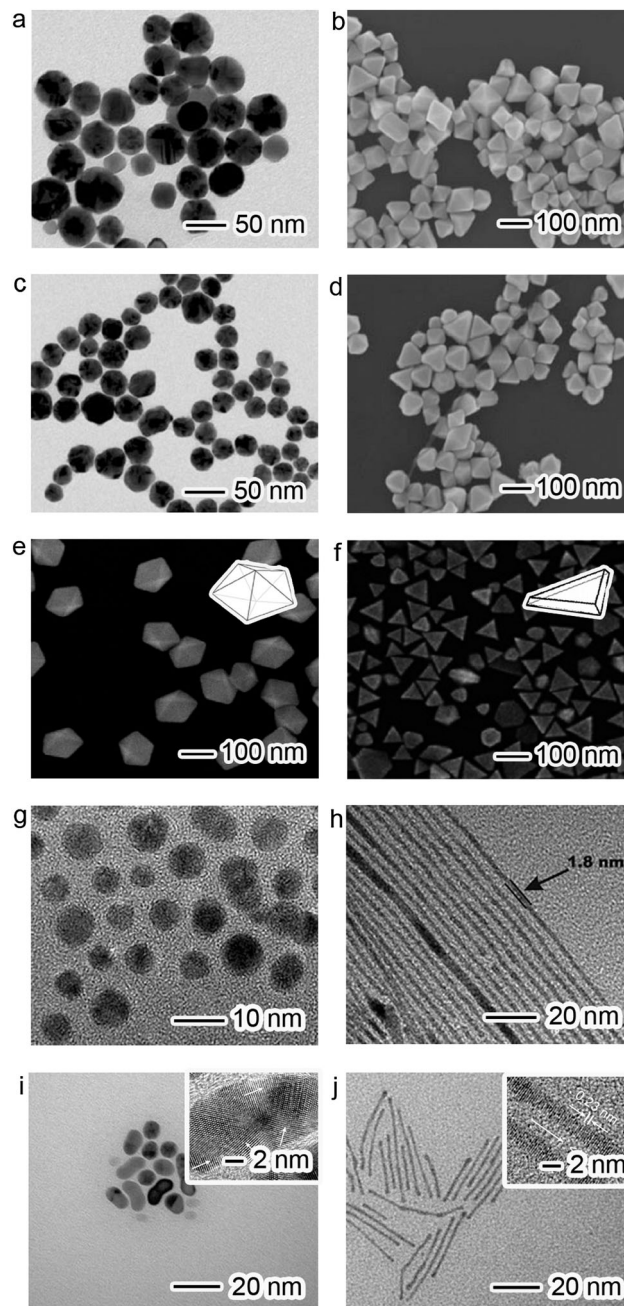


Fig. 5 TEM and SEM images of Au nanocrystals prepared in water in the presence of (a) low concentration of Cl⁻; (b) high concentration of Cl⁻; (c) moderate concentration of Cl⁻ under argon protection; and (d) moderate concentration of Cl⁻ fully exposed to oxygen (adapted with permission from ref. 81, Copyright 2010 Wiley-VCH Verlag GmbH & Co.). SEM images of Au nanocrystals prepared with HAuCl₄ and diethylene glycol (DEG) in the presence of PVP at (e) high concentration and (f) low concentration (adapted with permission from ref. 82, Copyright 2008 American Chemical Society). TEM images of Au nanoparticles prepared with AuCl in oleylamine and hexane: (g) in the absence of O₂ in the entire process; and (h) introducing O₂ during the later stages of the reaction (adapted with permission from ref. 54, Copyright 2011 Wiley-VCH Verlag GmbH & Co.). TEM images of Au nanostructures obtained in chloroform with Fe(III)/Fe(II) and O₂ (i) at 12 h; and (j) after 144 h (adapted with permission from ref. 83, Copyright 2008 American Chemical Society).

layer (e.g., oxide or polymer), the metals should be free of corrosion. Indeed, Song *et al.* found that poly(vinyl pyrrolidone) (PVP) can effectively protect the defects of multi-twinned nanocrystals against the etching by the Cl^-/O_2 pair. As a result, Au multi-twinned structures can be obtained at high concentrations of PVP (Fig. 5e), but are removed from the products when the concentration of PVP is low (Fig. 5f).⁸²

As the system switches to an organic medium, the situation becomes more complicated. For instance, when oleylamine is used as the solvent, the formation of oleylamine chains can contribute to the growth of Au nanowires.⁸⁵ However, Mourzina *et al.* found that the synthesis of Au nanowires in oleylamine strongly depended on the amount of O_2 in the reaction solution.⁵⁴ Oxidative etching plays a role in controlling the crystallinity of nanocrystals, which in turn guides the anisotropic growth of nanowires. In other words, it serves as a driving force to grow nanowires in addition to the function of oleylamine. As the reaction is performed under an inert atmosphere, Au nanoparticles with multiply twinned structures are produced due to the absence of etching (Fig. 5g). When oxygen is introduced into the system at the later stages, oxidative etching can remove oleylamine molecules from highly reactive twin-defect sites. During this process, Au is oxidized to Au(I) or Au(III) species, dissolving twinned structures and providing a feedstock of Au for growing single-crystal nanowires (Fig. 5h). Such a growth mode has also been observed in the synthesis of single-crystal Au nanorods with chloroform as a solvent in the presence of Fe(III)/Fe(II) and oxygen (Fig. 5i and j).⁸³ The key fact for this synthesis lies in the synergetic effects of oxidative etching (to dissolve twinned structures and generate fresh Au atoms) and atomic deposition (on single-crystal seeds for anisotropic growth), eventually reshaping the twinned nanocrystals into single-crystal nanorods or nanowires.

2.1.1.4 Cu. Cu nanostructures are of great interest in terms of their optical, electronic and catalytic applications, as the cost of this metal is orders of magnitude lower than Au, Ag, Pd and Pt. For example, Cu nanocrystals have tunable LSPR properties and SERS activities similar to Au. Cu nanowires can also be used for flexible, transparent conductive films. There is no doubt that future applications would greatly benefit from the synthesis of Cu nanostructures with well-defined and controllable parameters.

Cu can be easily oxidized and etched by Cl^- and O_2 . A typical example is the synthesis of Cu nanocubes developed by Jin *et al.* Similar to the Ag system, multiply twinned seeds are a favourable product in the synthesis. When the concentration of the capping agent hexadecylamine (HDA) is high, the HDA can prevent the twinned seeds from being oxidized and etched. As a result, they grow into multi-twinned nanowires (Fig. 6a). At low concentrations of capping agent, the multiply twinned seeds cannot survive oxidative etching, leaving the single-crystal nanocubes behind (Fig. 6b).⁸⁶

Given the difficulty in measuring and controlling the concentration of O_2 in the synthesis as well as the sensitivity of Cu to oxidation, the Cl^-/O_2 pair is not an ideal etchant in the

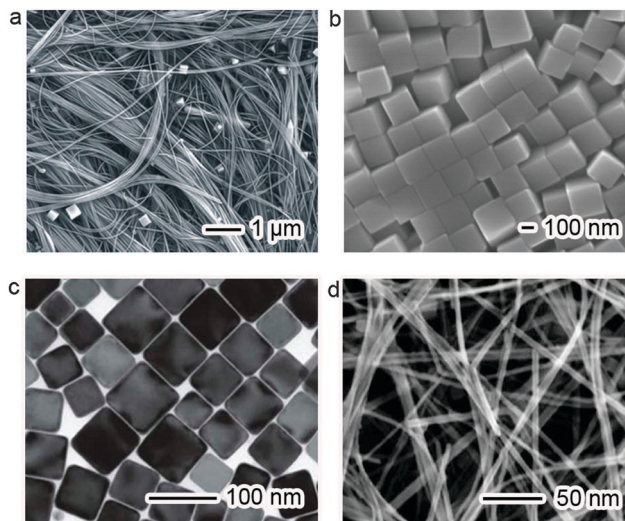


Fig. 6 SEM images of Cu nanostructures prepared in water with (a) 180 mg HDA and (b) 90 mg HDA (adapted with permission from ref. 86, Copyright 2011 Wiley-VCH Verlag GmbH & Co.). TEM and SEM images of Cu nanostructures prepared in oleylamine under protection of argon gas: (c) in the presence of TOP; and (d) in the absence of TOP (adapted with permission from ref. 87, Copyright 2013 Royal Society of Chemistry).

Cu synthesis. As an alternative, Peng *et al.* demonstrated that Cl^- and trioctylphosphine (TOP) could also serve as an etchant in the Cu alloy system, selectively etching the twinned structures. As a result, Cu nanocubes and nanowires can be selectively obtained, depending on the addition of TOP (Fig. 6c and d).⁸⁷

2.1.2 Size control. Particle size is one of the most important parameters with which the chemical and physical properties of nanocrystals have a strong correlation.¹ For instance, the LSPR band position, intensity and the scattering-to-absorption ratio of metal nanocrystals can be maneuvered by controlling their sizes.⁹⁰ In another important application of metals, the catalytic activities of metal nanocatalysts can be substantially enhanced when shrinking their dimensions due to the increased surface-to-volume ratios.¹⁶ For this reason, tremendous efforts have been made to tune the sizes of metal nanocrystals in various synthetic systems.

One of the commonly used methods for size control is to stop reactions and take samples out of the reaction solution at different stages of nanocrystals growth.^{67,91} This method cannot make full use of raw materials when stopping reactions in a short period to obtain small sizes. More importantly, it is known that the shape of metal nanocrystals evolves during their growth. For instance, in a typical synthesis of metal nanocubes, single-crystal seeds form cuboctahedral nanocrystals in the early stage, which then evolve into the nanocubes at relatively large sizes under the capping effects of PVP or other species. Thus the nanocrystals obtained by this method can have tunable sizes, but meanwhile possess varied geometries that may significantly impact their properties.

The seeding process is another approach to maneuvering the particle size by controllably adding metal atoms onto the surface of seeds.⁶⁴ In this process, seeds with well-defined

shapes are prepared in a synthesis, which are added into another solution for further growth after washing. Obviously, this two-step protocol is relatively complicated and its yield is limited by the low concentrations of seeds and chemicals that are required for the seeding process. In comparison, the method of oxidative etching can produce size-tunable nanocrystals in high yield and in consistent geometrical shapes.

In a typical example, Xiong *et al.* demonstrated the use of HCl as an effective etchant for size control.⁶⁶ In the early developed protocols, oxidative etching mainly works through O₂ and Cl in the reaction solution. However, many examples in literature indicate that oxidative etching by the Cl⁻ and O₂ alone is not strong enough to effectively etch single-crystal structures. According to the standard potential of O₂, the etching strength of Cl⁻ and O₂ can be dramatically enhanced by acid. Thus using HCl instead of NaCl or KCl can work better for the size control of single-crystal nanostructures.

Oxidative etching plays multiple functions in this size-controlled synthesis. First, it can effectively remove the twinned seeds, including both single-twinned and multi-twinned structures. Second, it oxidizes newly formed metal atoms back to ions, which constitutes a competition with the reduction of metal precursors. This competition substantially slows the nucleation

process, reducing the number of nuclei in the synthesis. At the same concentration and conversion yield of metal precursors, the sizes of final nanoparticles can be tuned by varying the numbers of nuclei (Fig. 7a and b). As a result, fewer nuclei will lead to larger sizes in the final products in a polyol synthesis of Ag nanocubes (Fig. 7c and d).

Based on the generic features of this approach, the use of HCl and O₂ as an etchant can be applied to other metals or various shapes. By increasing the concentration of HCl, the sizes of palladium nanocubes can be tailored from 8 to 20 nm in an aqueous synthesis (Fig. 7e and f). HCl and O₂ can also be used in the synthesis of palladium cuboctahedra to tune the size from 5 to 20 nm (Fig. 7g and h).⁶⁶ Xia and Xiong also demonstrated that Fe(III) species could serve as an etchant for size control by following a similar mechanism.⁹² It is worth noting that this size control method can keep the chemical environments of products consistent, advantageous to investigating their size-dependent properties and further applications.

2.1.3 Shape control. The interfacial energies of different surface facets play an important role in determining the shape of a nanocrystal. The formation of surface facets is essentially driven by total interfacial free energy. For fcc metals, the surface energies of low-index facets follow the sequence of $\gamma(111) < \gamma(100) < \gamma(110)$.

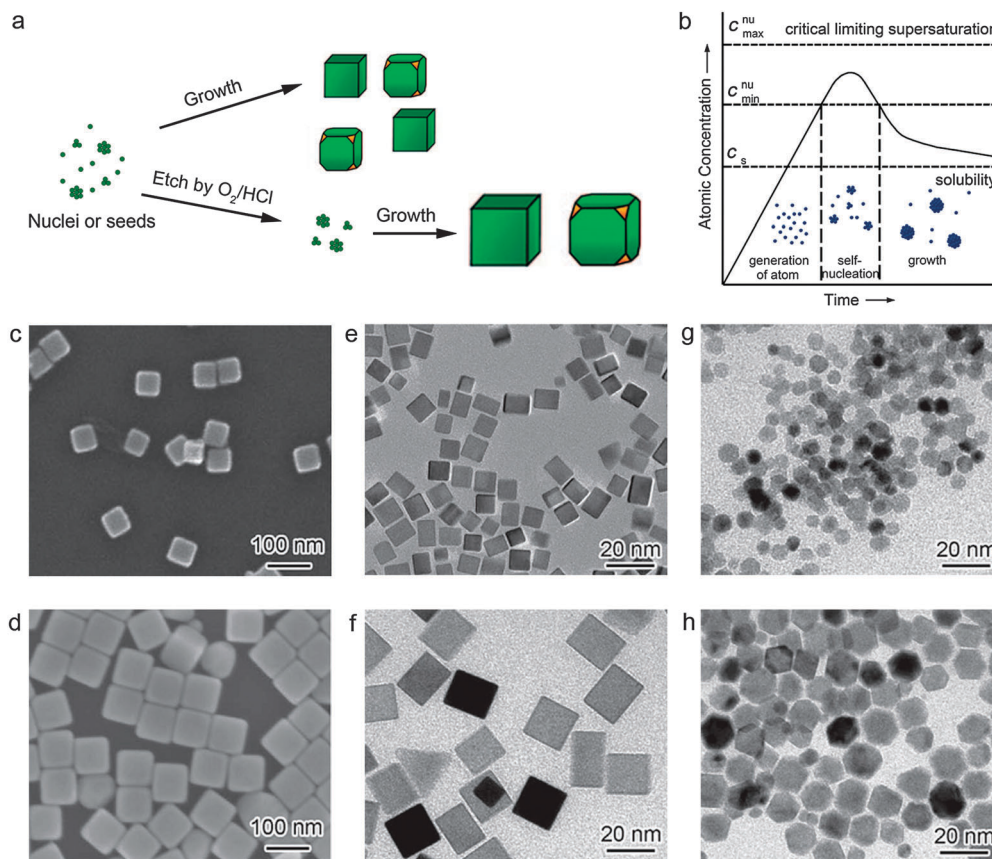


Fig. 7 (a) Schematic illustration for size control of metal nanocubes *via* oxidative etching. (b) Diagram for the atom generation, nucleation and subsequent growth (adapted with permission from ref. 1, Copyright 2009 Wiley-VCH Verlag GmbH & Co.). SEM images of silver nanocubes prepared in EG in the presence of different amounts of HCl: (c) 0.21 and (d) 0.28 mM. TEM images of palladium nanocubes prepared in water in the presence of HCl at different concentrations: (e) 0 and (f) 109 mM. TEM images of palladium cuboctahedra prepared in water in the presence of HCl at different concentrations: (g) 0 and (h) 218 mM (adapted with permission from ref. 66, Copyright 2012 Wiley-VCH Verlag GmbH & Co.).

Cuboctahedra (*i.e.*, quasi-Wulff polyhedra) have a nearly spherical profile with the smallest surface area to minimize their surface energies.¹ Multiply twinned structures are enclosed by $\{111\}$ facets having low surface energy, and their total free energy can be kept low despite the strain energy caused by their internal defects. As a result, both the cuboctahedral and multi-twinned particles can be favored by thermodynamics, depending on the size of the nanoparticle.⁶⁰ Other geometries of single-crystal and multi-twinned structures can be still obtained by modifying their surface energies by adding suitable capping agents onto the surface. This feature makes the use of capping agents a powerful tool to tailor the shape of metal nanocrystals. Essentially oxidative etching does not have distinct effects on the facet growth in a direct synthesis of nanocrystals.

In parallel, anisotropic growth represents another aspect for the shape control, leading to two types of anisotropic structures – one-dimensional nanorods (or nanowires) and two-dimensional nanoplates. In most cases, there is no intrinsic driving force for the growth of anisotropic structures when the reaction is under thermodynamic control, given the high symmetry of the fcc lattice. For the five-fold Ag nanowires (Section 2.1.1.1), the symmetry break is induced by the involvement of five-fold twin seeds. As the lateral growth of a decahedron would greatly

increase strain energy, the atoms prefer to being added along the axial direction parallel to the twin planes, leading to the elongation of the decahedron into nanowires.^{1,93} In this section, we highlight two other cases of anisotropic growth enabled by oxidative etching.

2.1.3.1 One-dimensional structure. As described above, the fcc metals have no intrinsic driving force for the growth of anisotropic structures when single-crystal seeds are surrounded by an isotropic medium. As dictated by thermodynamics, their atoms are expected to nucleate and grow into cuboctahedra to minimize the total surface energy. With capping agents used, particular facets dominate the surface of the nanocrystals. In most cases, the cubic symmetry of the fcc metal would not be broken by the addition of capping agents.

Xiong and Xia demonstrated that oxidative etching could selectively activate one side of single-crystal seeds to induce their anisotropic growth when the surface of seeds is passivated by certain species.³² Systematic studies suggest that the etching or corrosion on the seeds with passive surfaces starts with pitting corrosion (*i.e.*, occurs on a specific site).⁹⁴ This localized oxidative etching makes one face become more active than others and thus provides favorable sites for the addition of metal atoms (Fig. 8a–c).

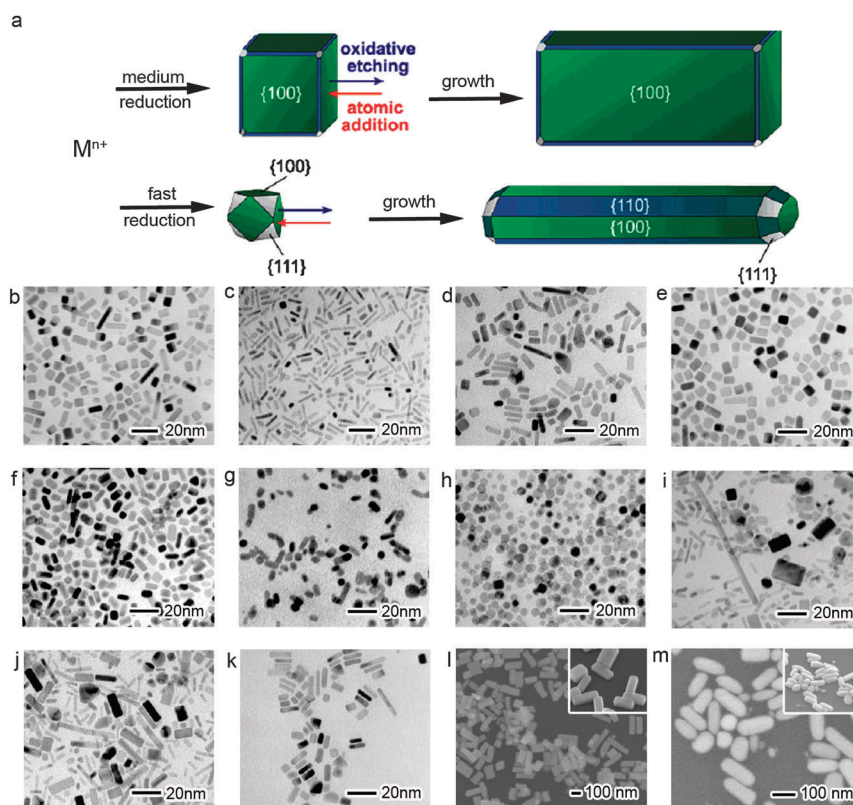


Fig. 8 (a) Schematic illustration of the mechanisms responsible for the anisotropic growth of single-crystal nanobars and nanorods. (b–i) TEM images of Pd nanocrystals synthesized in the presence of KBr in aqueous solution: (b) 9.1% EG in air; (c) 72.7% EG in air; (d) 72.7% EG in Ar; (e) 72.7% EG in air in the presence of 0.13 M citric acid; (f) 72.7% EG in air in the presence of 0.2 M NaCl; (g) 72.7% EG in air in the presence of 1 M HCl; (h–k) 72.7% EG in air but at different molar ratios of KBr to Na_2PdCl_4 (h, 0; i, 8; j, 15; k, 50) (adapted with permission from ref. 32, Copyright 2007 American Chemical Society). (l) SEM images of Ag nanobars prepared in EG in the presence of NaBr. (m) SEM images of Ag nanorices transformed from the nanobars (adapted with permission from ref. 88, Copyright 2007 American Chemical Society).

As long as the reduction kinetics is fast enough to supply sufficient Pd to the etched sites, atomic addition will be faster than the dissolution of atoms caused by the etching, resulting in anisotropic growth of seeds. This growth mode has been demonstrated with experiments that employed different etching strengths. For example, when the synthesis is protected from oxidative etching by Ar or citric acid (an agent able to remove oxygen as demonstrated in Section 2.1.1.2), the resultant products exhibit a decrease in aspect ratio compared to the ones obtained in air (Fig. 8d and e). On the other hand, when oxidative etching is enhanced by additional NaCl and HCl, it takes place over the entire surface of the seeds rather than locally on a specific face, also reducing the aspect ratio of Pd nanocrystals (Fig. 8f and g).

It is worth mentioning again that the passive surface of seeds is a prerequisite for selective etching. In the system shown above, bromide is used as a capping agent to promote the formation of {100} facets. More importantly, excessive capping of bromide on {100} facets can passivate the surface, inducing the selective etching on one face for anisotropic growth. However, it can be envisioned that the concentration of bromide has a more complicated impact on the system. The formation of complex ions $[\text{PdBr}_4]^{2-}$ alters the potential of Pd(IV) and thus the reduction kinetics. As the selective etching and fast reduction kinetics are both required for successful anisotropic growth, the highest aspect ratio of nanocrystals would be achieved with moderate concentrations of bromide in the reaction (Fig. 8h–k).

By implementing a similar strategy, Ag nanobars with an average aspect ratio of 2.7 have been made (Fig. 8l).⁸⁸ The reaction system involves PVP, AgNO₃ and NaBr without chloride. As demonstrated in the synthesis of Ag bipyramids,⁶⁹ bromide is an effective etchant in the synthesis of Ag nanocrystals given the high reactivity of Ag. Thus it can replace chloride with the same etching function. Interestingly, the nanobars can be transformed to nanorice (Fig. 8m) with round corners and edges by oxidative etching in air, offering the opportunity to tune their LSPR band (see Section 3).

2.1.3.2 Two-dimensional structure. Another way to break the symmetry is to make use of kinetic control. Certain structures such as nanoplates have significant stacking faults with noticeable strain energy, whose total free energy cannot be lowered to the level within the thermodynamic regime by any means. In the case that there is not enough thermal energy and/or time to reorganize the atoms on the surface of a particle to be in the thermodynamically favored state, the shape of the particle will be determined by the kinetics of nucleation and growth. As demonstrated by the structure and size control (see Sections 2.1.1 and 2.1.2), oxidative etching is a powerful tool to modulate the reduction and nucleation rate by continuously oxidizing freshly formed atoms back to ions. As such, the synthesis of nanocrystals may be turned into the kinetic control regime when the strength of oxidative etching is sufficient.

In such a case, as the reduction becomes extremely slow, atomic accumulation in the nucleation stage would lead to random hexagonal close packing (hcp) instead of fcc.^{19,89} In this way

stacking faults are incorporated into the nanocrystals, breaking the cubic symmetry. The strength of oxidative etching is a critical parameter to achieving effective kinetic control. Fig. 9a shows a schematic illustration for an etching window applicable to metals such as Ag and Pd that lead to the formation of two-dimensional structures. When the oxidative etching is implemented, the crystallinity of nanocrystals can be controlled by adjusting the strength of etching. As described in Section 2.1, five-fold twinned seeds can be etched due to their large lattice distortion even when the oxidative etching is relatively weak, while the single twinned seeds may survive. As the etching becomes stronger, the single twinned seeds no longer sustain the oxidative attack, leaving single-crystal seeds behind. With the strength further enhanced, the oxidative etching can serve as a promising approach to kinetic control. On the other hand, oxidative etching can effectively prevent the formation of multiply twinned structures so as to ensure the purity of kinetically controlled products – nanoplate with stacking faults.

The formation of these planar defects in two-dimensional nanoplates is determined by the balance between the repulsive force (between dislocations) and attractive force (surface tension).^{96,97} Stacking fault energy (SFE) is a parameter for this balance, whose value reflects whether the stacking faults can be easily formed. Pt is a metal with very high SFE, which makes its stacking-fault structures extremely unstable and hardly achievable. For other metals, as long as the synthesis falls into kinetic control regime, the atoms are allowed to stack into the hcp structure.^{96,97} Once the hcp structures are formed and grow larger, they become stable with surface energies lowered by the large {111} surfaces, and can survive in a strong etching environment.

Taken together, the oxidative etching can make the nanoplates become a major product in a kinetically controlled regime (Pt is an exception that will be discussed in next section).⁹⁸ Several research groups have employed oxidative etching as a kinetic control tool to obtain high-quality triangular, hexagonal and circular nanoplates of many metals.^{19,89,95} In a typical example, Yin *et al.* yielded Ag nanoplates with various Ag sources including Ag salts and metallic Ag by harnessing the oxidative etching power of H₂O₂ (Fig. 9b and c).⁸⁹ As a universal rule, this kinetic control brought about by oxidative etching can be applied to other metals. As is well known, the use of HCl and O₂ as an etchant can remove twinned structures in the synthesis of Pd nanocrystals. With Fe(III) species combined with HCl and O₂, the reduction kinetics of the Pd precursor can be significantly altered to yield Pd nanoplates.¹⁹ During the growth of nanoplates, there is a typical evolution process from hexagonal to triangular profiles. Thus a delicate control of the etching strength can tune the growth of nanoplates into various profiles. When the strength of oxidative etching is not so strong, the reaction rate is relatively high so that the synthesis directly goes to final stage of shape evolution – the formation of triangular nanoplates (Fig. 9d). By doubling the amount of FeCl₃, the reduction kinetics is further slowed so that the intermediate growth stage can be captured. As a result, hexagonal nanoplates which represent another kinetically controlled morphology can be obtained (Fig. 9e).

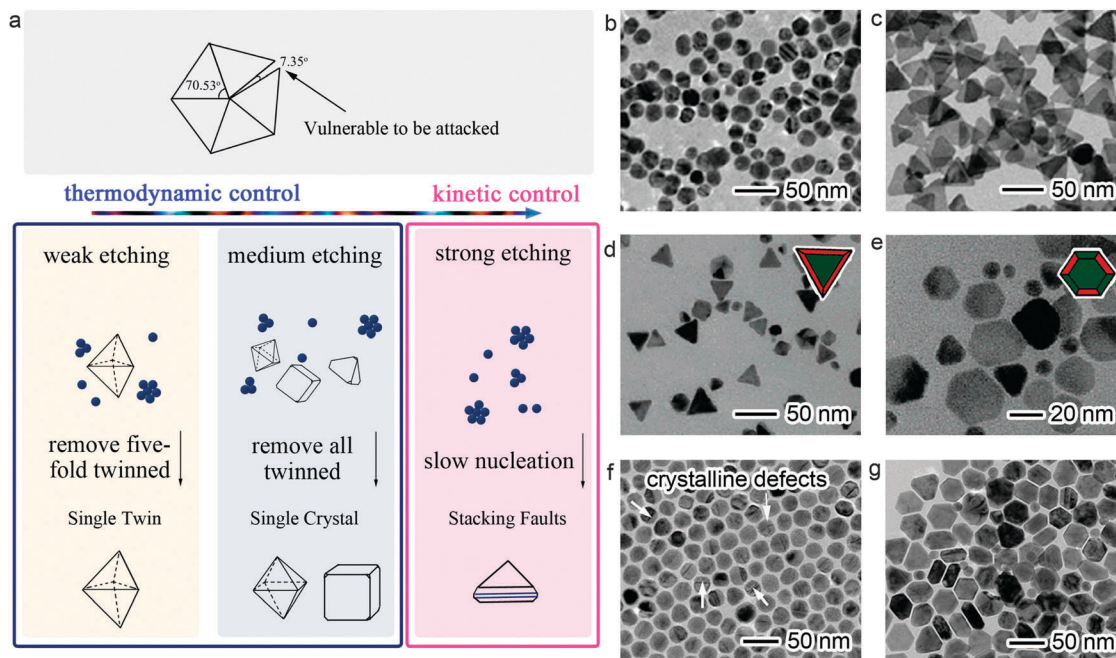


Fig. 9 (a) Schematic illustration of the mechanisms involved in etching-controlled syntheses. TEM images of (b) Ag nanoparticles prepared in the presence of PVP; (c) Ag triangular nanoplates prepared in the presence of PVP, citrate and H_2O_2 (adapted with permission from ref. 89, Copyright 2011 American Chemical Society); (d) Pd triangular nanoplates prepared in the presence of 0.36 mM FeCl_3 and 5 mM HCl; (e) Pd hexagonal nanoplates prepared in the presence of 0.72 mM FeCl_3 and 5 mM HCl (adapted with permission from ref. 19, Copyright 2005 American Chemical Society); Ni-Cu alloy nanoparticles prepared in oleylamine at different time intervals: (f) 15 min and (g) 30 min (adapted with permission from ref. 95, Copyright 2012 Royal Society of Chemistry).

The kinetics of synthesis can also be controlled by oxidative etching in organic media. A typical demonstration is the synthesis of Ni-Cu alloy nanoplates in oleylamine. As compared with other metals, the Ni-Cu alloy can be more easily oxidized. Peng *et al.* demonstrated that oxidative etching could still work with the chloride in CuCl_2 together with oleylamine and TOP even when the synthesis was performed under the protection of argon, leading to the formation of nanoplates (Fig. 9f and g).⁹⁵

Overall, the metal nanocrystals that are not favored by thermodynamics (*e.g.*, nanoplates) can be readily synthesized with high quality, when the concept of kinetic control is fully understood and combined with the tool of oxidative etching. It provides a conceptually new approach to shape control with universal capabilities as well as a platform to enable fascinating properties and applications.

2.1.3.3 Exception – high SFE material (Pt). Pt has been widely utilized as a catalyst in catalytic converters, oil cracking and proton-exchange membrane (PEM) fuel cells.⁹⁹ However, the low abundance and high price of Pt is a major limitation to its continued use. One way to potentially make better use of Pt is to design Pt nanostructures that optimize the catalytic activity of the material.

Oxidative etching can play a special role in controlling the structures of seeds in the Pt system in contrast to other metals. The fcc accumulation mode is much more favorable than rhcp in Pt system based on the DFT-LDA calculation results.¹⁰⁰ This feature determines that the twinned crystal structures are rarely

formed in Pt nanocrystals. Unlike Ag, Au and Pd cases, the SFE of Pt is rather high (Table 3), which makes the stacking faults of Pt quite unstable.⁹⁷ Thus, even in the case that the rhcp structures of Pt can be formed at the early nucleation stage, they will be easily dissolved by the oxidative etching.

Other than this function (see Fig. 10a and b), it can play a more sophisticated role as recently demonstrated in a one-step synthesis of branched Pt nanocrystals.⁴⁹ This method offers the possibility of tuning the numbers of branches and high-index facets in a single system without the need for altering capping agents, and enables the reliable evaluation of structure-dependent catalytic performance free of surface chemistry interference. In this system, demonstrated by Xiong *et al.*, Pt nanocrystals are grown in a reaction system where H_2PtCl_6 , PVP and KBr are dissolved in a mixed solvent of ethylene glycol and water. In the presence of oxygen, different amounts of HCl are added to the reaction system to tune the crystallinity of the seeds (*i.e.*, twinned *versus* single-crystal, Fig. 10a and b) and the modes of atomic addition (*i.e.*, sites and rates for atomic addition, Fig. 10c). Basically the acidity of HCl can greatly enhance the etching strength of Cl^- and O_2 .⁶⁶ TEM studies in different stages reveal that the tripods are formed from the single-twinned seeds while the tetrapods, hexapods and octopods all evolve from the single-crystal cuboctahedral seeds (see Fig. 10d–g). In addition to controlling the structures of seeds, oxidative etching has also demonstrated its functions in modulating atomic addition through: (1) the crystallinity of seeds; (2) the faces that are activated on the seeds for atomic addition; (3) the

Table 2 Summary of etching conditions correlated with product structures in a direct synthesis

Etchants	Concentration of etchants ^a	Crystallinity	Shape of final products	Ref.	
Ag	None	—	Multi-twinned	Twinned nanoparticles	60
	Br ⁻ /O ₂	0.03 mM (NaBr)	Single-twinned	five-fold twinned nanowire	69
		0.06 mM (NaBr)	Single-crystal	Right bipyramid	88
	Cl ⁻ /O ₂	0.06 mM (NaCl)	Single-crystal	Nanobars	60
	HCl/O ₂	0.25 mM (HCl) or 0.21–0.35 mM (HCl)	Single-crystal	Nanospheres nanocubes	62 and 66
	H ₂ O ₂	20 mM	Stacking faults	Nanoplates	89
	Fe(III)/Fe(II)	2.2–22 μM	Single-crystal	Nanocubes	63
		0.44 μM	Multi-twinned	Twinned nanoparticles	63
				five-fold twinned nanowires	
	Cu(II)/Cu(I)/Cl ⁻	1.4 × 10 ⁻⁷ mM (CuCl ₂)	Single-crystal	Cubes, cuboctahedra octahedra	64
		19.9 μM (CuCl ₂)	Multi-twinned	Twinned nanoparticles	68
				five-fold twinned nanowires	
Au	Cl ⁻ /O ₂ (reaction time included)	0–7.2 mM (CTAC)	Multi-twinned	94% icosahedra	81
		14.4 mM (NaCl)	Single-crystal twinned	22% octahedra twinned nanoparticles	
		14.4–28.8 mM (CTAC)	Mostly single-crystal	85% octahedra 15% truncated bipyramids	
		2.1 mM ([AuCl(OLA)]); 0–96 hours	Multi-twinned	Multi-twinned nanoparticles multi-twinned nanorods	83
		2.1 mM ([AuCl(OLA)]); 144–196 hours	Single-crystal	Single-crystal nanorods	
	Cl ⁻ /O ₂ (concentration of capping agent included)	7.2 mM (HAuCl ₄); 0.62 mM (PVP)	Multi-twinned	Decahedra	82
		7.2 mM (HAuCl ₄); 0.03 mM (PVP)	Single-crystal	Icosahedra truncated tetrahedra	
Cu	Cl ⁻ /O ₂ (concentration of capping agent included)	24.6 mM (CuCl ₂); 0.07 mM (HDA)	Multi-twinned	Twinned nanowires	86
		24.6 mM (CuCl ₂); 0.04 mM (HDA)	Single-crystal	Nanocubes	
	Cl ⁻ /TOP	0.2 M (CuCl ₂); no TOP	Multi-twinned	Twinned nanowires	87
		0.2 M (CuCl ₂); 143 mM TOP	Single-crystal	Nanocubes	
Pd	None	—	Multi-twinned	Twinned nanoparticles	48
	O ₂	—	Single-crystal	Cuboctahedra	48
	Br ⁻ /O ₂	0.17–0.45 M (KBr)	Single-crystal	Nanocubes	55 and 16
		0.46 M (KBr)	Single-crystal	Nanorods	32
	HCl/O ₂	0.21–0.35 M (HCl)	Single-crystal	Nanocubes cuboctahedra	66
	I ⁻ /O ₂	0.17 M (NaI)	Single-twinned	Right bipyramids	55
		0.67 M (NaI)	Single-crystal	Nanocubes	55
Pt	None	—	Stacking faults	Tripods	49
	HCl/O ₂	112.5–337.5 mM (HCl)	Single-crystal	Tetrapods, multipods	49

^a The concentration was calculated in final reaction solution.

rate of atomic addition. Taken together, these three functions of oxidative etching can tune the nucleation and growth modes to generate Pt nanocrystals with different numbers of branches.

In this section, oxidative etching has clearly demonstrated its function as a powerful tool that can attack the defects of

twinned seeds and turn the undesired atoms back into ions. It allows us to manipulate the crystallinity of products between twinned structures and single crystals as well as the way that the atoms are added to the seeds (refer to Table 2). Elucidating the exact mechanisms behind these processes will undoubtedly improve the controllability over metal synthesis at the nanoscale.

Table 3 Stacking fault energies (mJ m⁻²) for fcc metals: γ_{us} (stacking fault nucleation barrier), γ_{isf} (one-layer SFE)⁹⁷

Metal	γ_{us}	γ_{isf}	Expt.
	Theory	Theory	
Ag	133	18	16
Au	134	33	32
Cu	180	41	45
Ni	273	110	125
Pd	287	168	180
Pt	339	324	322

2.2 Oxidative etching in nanocrystals

Once the nucleation and growth are completed, the synthesis will produce nanocrystals with given geometries. However, not all desired shapes and structures can be generated in a direct growth step. In this case, one can carve the nanocrystals into another shape. Oxidative etching has demonstrated its ability to modify the shapes and structures of nanocrystals *via* atomic subtraction and addition. In terms of the etching process, it prefers to occur on defects of the nanocrystals such as twinned planes.

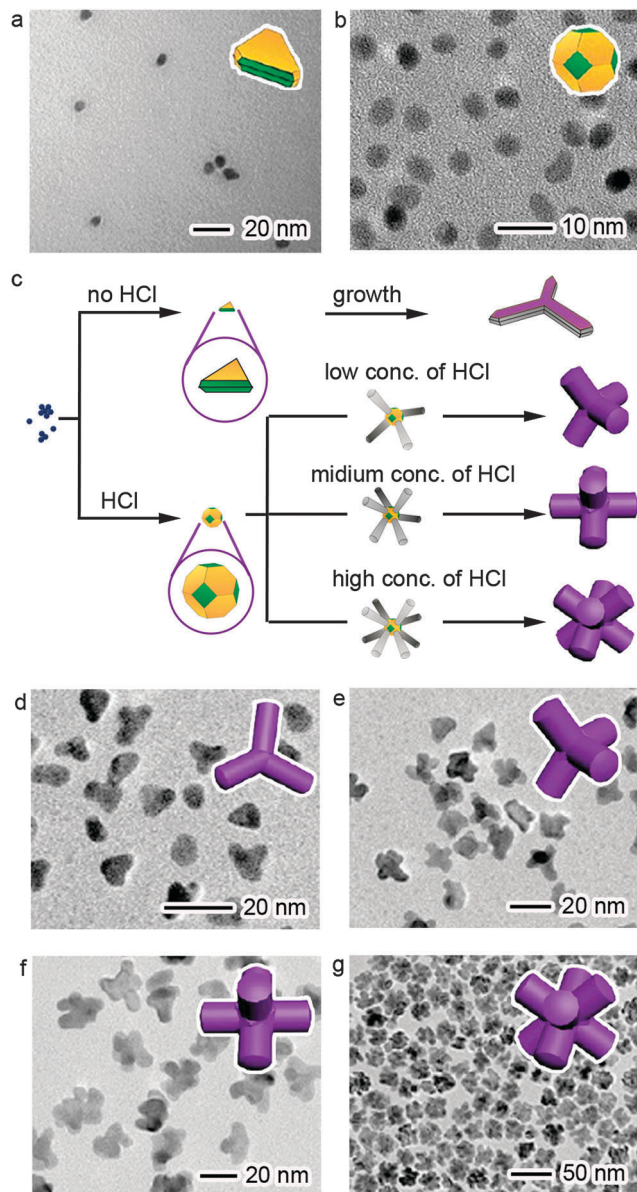


Fig. 10 TEM images of Pt seeds formed in air: (a) in the absence of HCl at 30 min; and (b) with 225 mM HCl at 15 min. (c) Schematic illustrating the growth of various branched nanocrystals. TEM images of Pt nanocrystals prepared in air in different amounts of HCl: (d) in the absence of HCl at 24 h; (e) with 112.5 mM HCl at 24 h; (f) with 225 mM HCl at 24 h; and (g) with 675 mM HCl at 24 h (adapted with permission from ref. 49, Copyright 2012 American Chemical Society).

Other than that, the corners and edges of a nanocrystal are the locations where oxidative etching can easily attack because of their high reactivity. Last but not least, isotropic etching happens on the entire surface of nanocrystals once the most active sites have been etched. Certainly this situation depends on the surface chemistry of nanocrystals. In practice, capping agents are generally involved in the synthesis of metal nanocrystals, and as a result, the nanocrystal surface is not clean but covered by some molecules or ions. The species on the surface will affect the etching process, and in turn, the possible atomic addition

accompanied by etching. The interplay between the surface chemistry of a nanocrystal, capping agents, and etchants offers lots of opportunities to design an etching process to reshape nanocrystals after the initial growth step.

2.2.1 Atomic subtraction. In contrast to atomic addition during the growth of nanocrystals, the removal of atoms by oxidative etching is a process of atomic subtraction. By applying atomic subtraction to existing nanocrystals, the library of nanocrystal shapes and structures can be further enriched. In this section, we will discuss two types of atomic subtraction – digging inside or carving outside – to produce new geometries.

2.2.1.1 Digging inside. In order to fabricate single-crystal hollow structures, one straightforward strategy is to dig inside solid nanocrystals and remove their interior materials. For instance, nanocubes can be an ideal platform for oxidative etching by the Cl^- and O_2 pair to make single-crystal nanoboxes and nanocages (Fig. 11a and b).¹⁰¹ However, oxidative etching occurs all over the surface in most cases, eventually leading to the total dissolution of nanoparticles. To remove the interior of a nanocrystal, one can use pitting corrosion. In a typical process, a high concentration of PVP is used to tightly surround and passivate the nanocubes. As a result, etching by Cl^- and O_2 has to start locally to make some pits (Fig. 11c). As the etching continues, the interior of each cube becomes increasingly empty. Meanwhile, the holes on the surface start to shrink due to the reduction of Pd(II) (originating from the dissolved Pd during the etching) and deposition of Pd atoms, producing perfect hollow nanoboxes (Fig. 11d). As the etching proceeds, small holes appear at the corners of each nanobox, thus turning the nanobox into a nanocage (Fig. 11e).

Another approach is based on the atomic subtraction on bimetallic nanostructures.⁵⁶ In this approach, Pd–Rh concave nanocubes with a core–frame structure are first prepared through a seeding process (Fig. 11g and h). With oxidative etching, the cores of Pd nanocubes can be removed to leave Rh cubic nanoframes (Fig. 11i and j). Oxidative etching in this system is accomplished with the combination of H^+ , Fe(III) and Br^- . The reduction potential of Fe(III)/Fe(II) is 0.771 V (vs. the standard hydrogen electrode), so the Fe(III) can be an effective etchant for Pd particularly in the presence of bromide and acid. Further, the bromide facilitates the etching on Pd due to the formation of the $[\text{PdBr}_4]^{2-}$ complex, while the acid can enhance the etching strength.

2.2.1.2 Carving outside. Carving the surface is a more general approach to reshaping nanocrystals *via* oxidative etching. The consequence of carving outside varies with the chemical environment around the nanocrystals, since it can alter the locations and rates of oxidative etching. In fact, oxidative etching on nanocrystal surfaces that induces morphological changes has been widely observed for Ag, Au and Pd. A typical example is the shape evolution of various nanocrystals associated with their stability, triggered by oxidative etching. The nanocrystals spontaneously evolve into the shapes that are more favored by thermodynamics, no matter whether the nanocrystals are stabilized by capping agents or obtained *via* kinetic control.

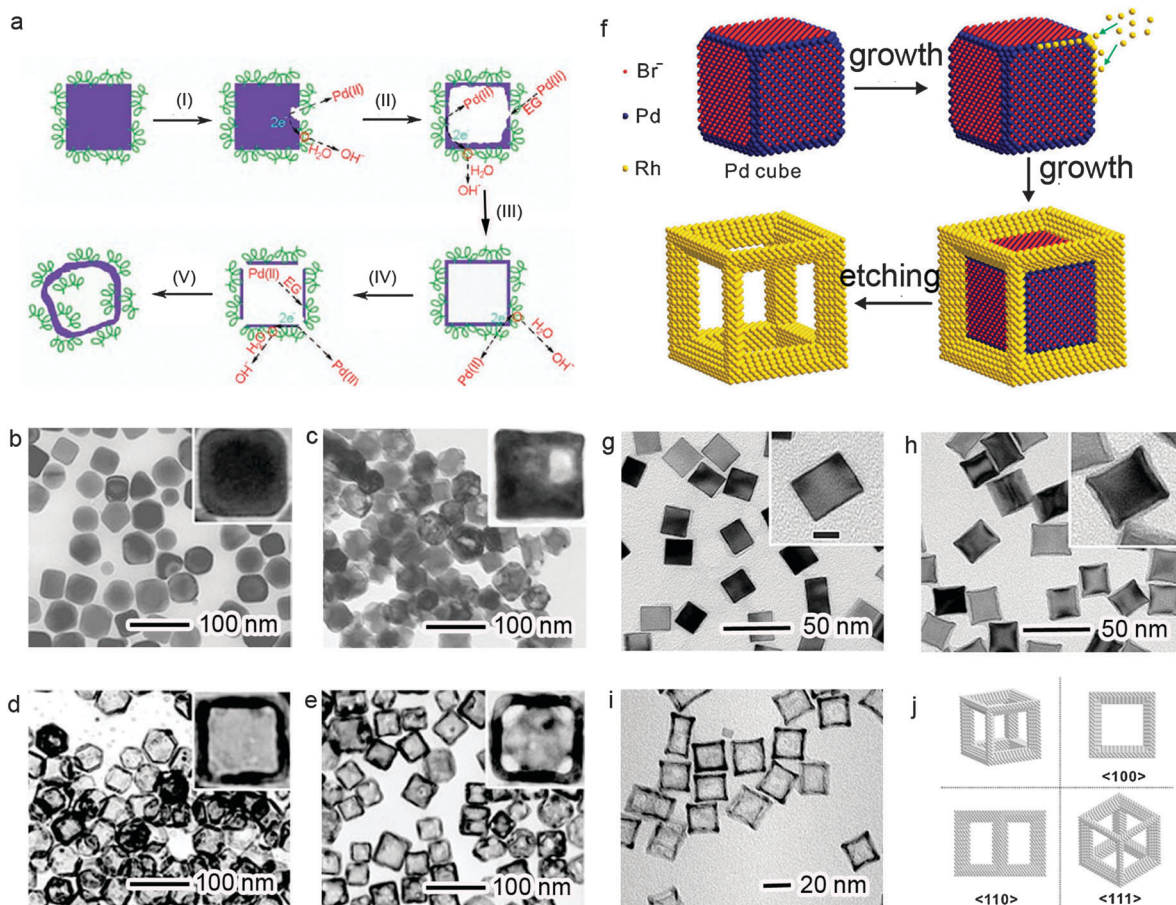


Fig. 11 (a) Schematic illustration of the transformation of solid nanocubes into hollow structures caused by oxidative etching: (I) pitting at a specific site on the surface of a nanocube; (II) formation of a hollow structure after further etching; (III) formation of a completely enclosed nanobox; (IV) formation of a corner-dissolved nanocage; (V) collapse of the nanocage. TEM images of Pd nanostructures in the presence of PVP, Na_2PdCl_4 , water and EG at different reaction stages: (b) $t = 18$ h; (c) $t = 20$ h; (d) $t = 22$ h; (e) $t = 24$ h (adapted with permission from ref. 101, Copyright 2005 Wiley-VCH Verlag GmbH & Co.). (f) Schematic illustration summarizing the three major steps involved in the synthesis of Pd–Rh core-frame concave nanocubes and Rh cubic nanoframes. TEM images of Pd–Rh core-frame concave nanocubes with different amounts of Na_3RhCl_6 : (g) 2.5 mg and (h) 10 mg. (i) TEM image of Rh cubic nanoframes obtained by selectively etching away the Pd cores. (j) A 3D model of Rh cubic nanoframe and its projections along $\langle 100 \rangle$, $\langle 110 \rangle$ and $\langle 111 \rangle$ zone axes (adapted with permission from ref. 56, Copyright 2012 Wiley-VCH Verlag GmbH & Co.).

This phenomenon has been commonly recognized in the literature, including the transformation of nanocubes to cuboctahedra and triangular nanoplates to circular ones.^{29,32}

This shape evolution can be facilitated by oxidative etching. For instance, Ag nanocubes can be transformed into nanospheres by etching their corners and edges with $\text{Fe}(\text{NO}_3)_3$ in a very short period of time (*i.e.*, 10 min, see Fig. 12a–d).¹⁰² With the capping PVP replaced with citric acid, the $\{100\}$ facets of nanocubes cannot be stabilized any more so that their transformation into the nanospheres becomes much easier.³¹ Even in the absence of strong etchants, this transformation can be accomplished by etching with oxygen.

A similar etching-induced shape evolution has been observed on Au icosahedra. Zhang *et al.* found that truncated icosahedral (football-shaped) Au nanocrystals can be obtained by etching icosahedral nanocrystals (Fig. 12e–h).¹⁰³ The function of oxidative etching has been verified by the experiment with citric acid – a typical agent to prevent oxidative etching as

previously demonstrated. When the starting materials switch to Ag octahedra, they can be etched by an etchant solution of NH_4OH and H_2O_2 (9:1). It induces the removal of corners and edges from the octahedra, and eventually leads to the formation of octopod-shaped nanocrystals (Fig. 12i–l).¹⁸

This etching-reshaping scheme is not limited to isotropic structures. In the case of Au nanorods, oxidative etching in the presence of $\text{Fe}(\text{III})/\text{Fe}(\text{II})$ and cetyltrimethylammonium bromide (CTAB) leads to a significant decrease in their length while their diameter is largely maintained (Fig. 12q–t).¹⁰⁴ This length reduction by oxidative etching can also be achieved with the etchants of HCl ¹⁰⁵ and CuCl_2 .¹⁰⁶ From the analysis above, one can see that all the shape evolution is carried out by oxidative etching, but is essentially driven by thermodynamic control to lower the total interfacial free energy. Apparently cutting the corners/edges of a nanocrystal (as well as the length of a nanorod) can minimize its surface area to reach a lower energy level.

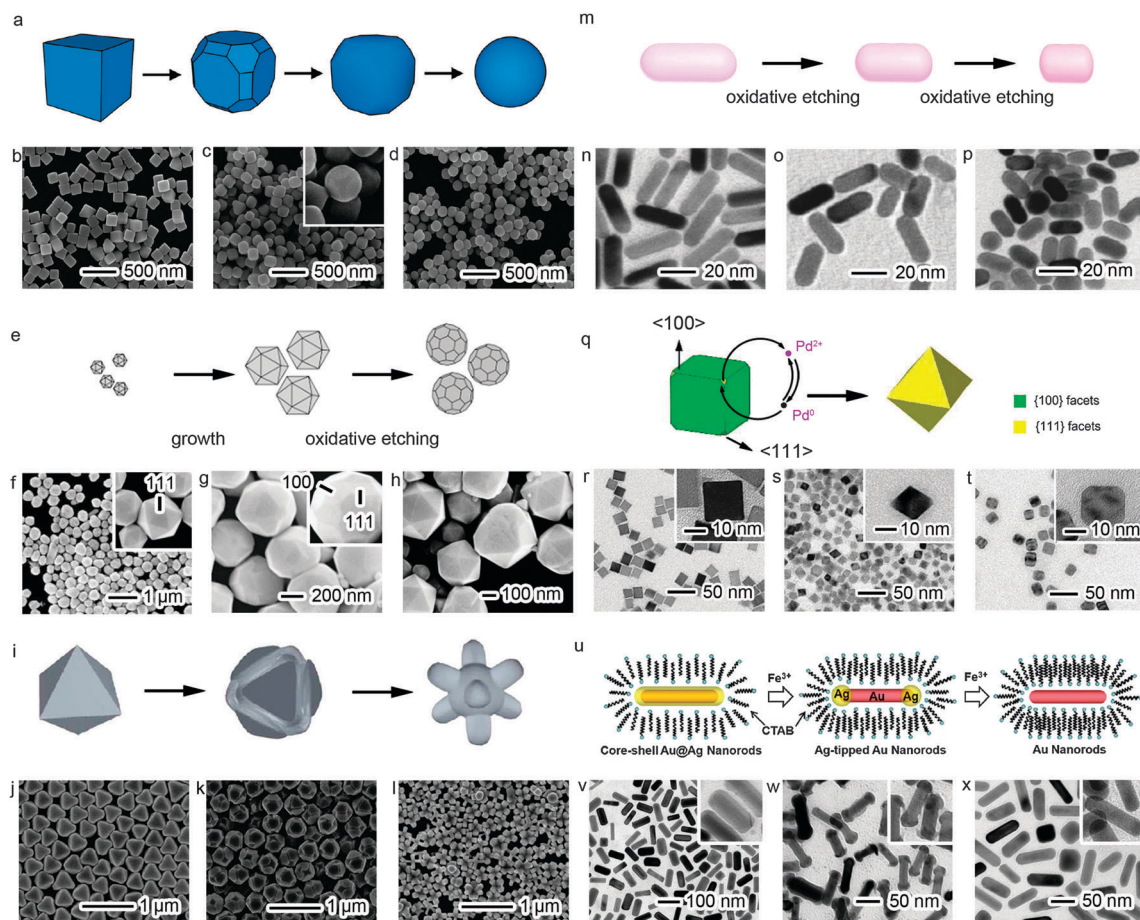


Fig. 12 (a) Schematic illustration of oxidative etching working on Ag nanocubes. SEM images of (b) Ag nanocubes, (c) Ag truncated nanocubes obtained by etching the sample b, and (d) Ag nanospheres by excessively etching the sample c (adapted with permission from ref. 102, Copyright 2009 American Chemical Society). (e) Schematic illustration of oxidative etching working on Au icosahedra. SEM images of (f) Au icosahedra, (g) Au truncated icosahedra obtained by etching the sample f, and (h) the sample made under the same conditions as (g) except that the etching was retarded by 0.1 mM citric acid (adapted with permission from ref. 103, Copyright 2008 Wiley-VCH Verlag GmbH & Co.). (i) Schematic illustration of oxidative etching working on Ag octahedra. SEM images of (j) Ag octahedra, (k) the sample j with edges/corners etched, (l) the octopods made by excessively etching the sample j (adapted with permission from ref. 18, Copyright 2010 American Chemical Society). (m) Schematic illustration of oxidative etching working on Au nanorods. TEM images of Au nanorods etched in the presence of 55 mM FeCl_3 and 2 mM CTAB for (n) 0 min, (o) 1 h, and (p) 5 h (adapted with permission from ref. 104, Copyright 2009 Royal Society of Chemistry). (q) Schematic illustration summarizing the major steps involved in the oxidative etching and regrowth process. TEM images of (r) Pd nanocubes of 18 nm in edge length and (s) Pd octahedron of 13 nm in edge length that were prepared by etching with 180 μmol HCl. (t) Pd nanocrystals that were prepared by etching with 60 μmol HCl without O_2 (adapted with permission from ref. 107, Copyright 2013 American Chemical Society). (u) Schematic illustration of etching on Au@Ag core-shell nanorods induced by FeCl_3 . TEM images of (v) Au@Ag core-shell nanorods, (w) partially etched structures, (x) completely etched structures (adapted with permission from ref. 52, Copyright 2012 American Chemical Society).

When the system involves nanocrystal growth in addition to the etching, the story becomes much more complicated. For instance, Pd nanocubes are a class of nanocrystals whose $\{100\}$ facets are covered by bromide.^{16,32} Due to this unique surface chemistry, Pd atoms are selectively removed from corners during oxidative etching by HCl- O_2 pair, making $\{111\}$ facets appear. The resultant Pd(II) can be again reduced and deposited back onto the nanocrystals with a preference for their $\{100\}$ facets, constituting a regrowth process. The etching to enlarge the $\{111\}$ together with the regrowth to diminish the $\{100\}$ facets leads to the formation of Pd octahedra (Fig. 12q-s).¹⁰⁷ Depending on the ratio of etching to regrowth, controllable edge lengths can be achieved on the octahedra. By varying the

added amount of HCl, the rate of etching can be readily tuned. At a low concentration of HCl, atomic subtraction and addition make equal contributions to the formation of Pd octahedra. When the strength of oxidative etching is enhanced by increasing the HCl amount, the atomic subtraction will take the leading role. As a result, the size of Pd octahedra can be tuned between 13 and 23 nm. Apparently, the absence of any component in the etchant pair would not lead to the formation of octahedra (Fig. 12t).

Further, the tool of oxidative etching can be extended to bimetallic materials. Taking advantage of the difference between metals in resistance to oxidative corrosion, it is feasible to employ the etching tool to synthesize bimetallic structures with different hybrid configurations. Yang *et al.* found that Fe(III)

and Br^- can be used to etch the Ag in Au@Ag core-shell nanorods, providing an approach to coating the entire nanorods with Ag or leaving Ag on their tips (Fig. 12u-x).⁵² This synthetic strategy has been extended to the synthesis of Pd-tipped Au nanorods.

Overall, corrosion of metals is a natural phenomenon caused by oxygen and corrosive ions. Although it is usually viewed as a detrimental process that destroys the usefulness of tools and machines, the oxidative corrosion has been identified as a simple, elegant and powerful method for reshaping the nanocrystals into various interesting geometries that cannot be achieved in a direct synthesis.

2.2.2 Atomic addition. Atomic addition controlled by oxidative etching is a complex and dynamic process. During this process, both the generation of atoms by reduction and dissolution of atoms by oxidation take place. In general, the reduction should be faster than the oxidation to enable atomic addition, but oxidative etching is necessary and decisive to the shape evolution of nanocrystals. In most cases, this process starts with atomic subtraction, followed by controllable atomic addition. The locations where oxidative etching occurs basically determine the sites for atomic addition during the further reduction process. This high selectivity brings prospects to further engineering nanocrystals towards the desired structures.

Cubic nanocrystal is a clear and simple structure that can serve to illustrate the role of oxidative etching in shape evolution. As demonstrated in Section 2.2.1.2, oxidative etching prefers to occur on the corners and edges of a nanocube. This etching effect was recently identified as a trigger to induce significant shape evolution *via* atomic addition (Fig. 13a).⁵¹ In a sulfide-mediated synthesis of Ag nanocubes, it is known that mild etching is present in the late stages. From TEM analysis, it has been identified that approximately 20% of nanocubes appear to have one truncated corner (Fig. 13b). Further, the etching on this corner will promote the atomic addition to all three adjacent faces that share this corner, leading to a unique anisotropically truncated octahedral shape (Fig. 13c). When the reaction is performed in Ar, it does not undergo any shape transformation, supporting the argument that the atomic addition is induced by the etching.

A similar process can be applied to create concave structures. In a traditional growth of Pd nanocubes into concave structures, lateral size of nanocrystals significantly increases from 17 nm to 33 nm.¹⁰⁸ The increase in particle size largely limits the performance of these structures as catalysts. When oxidative etching is employed with a seeding process, epitaxial growth with the capability of preventing atomic addition on undesired locations can be achieved (Fig. 13d). In this process, the corners and edges of nanocubes are first activated *via* the etching by HCl and O_2 . With the faces protected from atomic addition by bromide, further Pd and Pt epitaxial growth has no choice but to occur on the activated sites to generate Pd and Pd-Pt concave nanocubes (Fig. 13e and f).⁷⁶

With the development of controllable oxidative etching, one can manipulate atomic addition to preferentially occur on the activated sites, particularly on corners and edges of a nanocrystal. However, this atomic addition controlled by oxidative etching

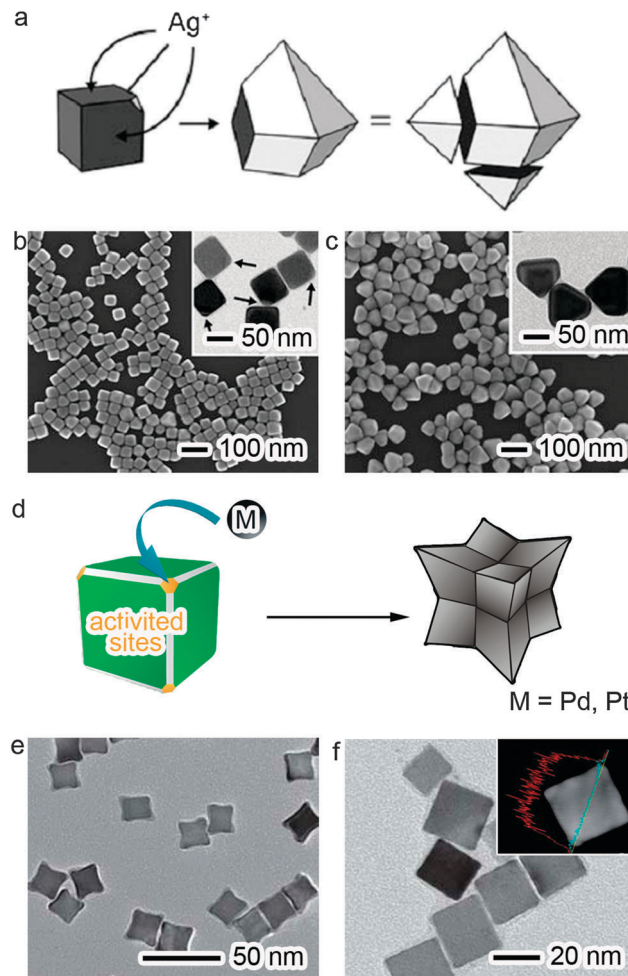


Fig. 13 (a) Schematic illustrating the unsymmetrical growth of a cubic seed. SEM images of (b) corner-etched Ag nanocubes, and (c) anisotropically truncated Ag octahedra (adapted with permission from ref. 51, Copyright 2009 Wiley-VCH Verlag GmbH & Co.). (d) Schematic illustrating the selective activation and atomic addition on the corners and edges of a nanocube. TEM images of (e) Pd concave nanocubes prepared with HCl surface activation and epitaxial growth, and (f) Pd-Pt nanocubes obtained *via* HCl surface activation and Pt epitaxial growth (adapted with permission from ref. 76, Copyright 2013 Royal Society of Chemistry).

is still in the early stage of development, calling for further investigations along this direction.

2.4 Common etchants and protection agents for oxidation etching

Wrapping up the recent developments, we list the frequently used etchants whose components include but are not limited to: O_2 , H_2O_2 , Fe(III)/Fe(II) , Cu(II)/Cu(I) , Br^- , Cl^- , and H^+ . The common methods to block or retard oxidative etching are: inert gas protection and addition of protection agents such as citric acid (see Table 4).

Among various etchants, Cl^- and O_2 are the most widely used. It takes little to no effort to introduce the oxygen in air into a reaction. Chloride ions are commonly contained in many metal precursors, can easily be added, and are often present as

Table 4 Summary of common etchants and protection agents in the oxidative etching process on common metals

	Ag	Au	Cu	Pd	Pt
Cl ⁻	Etchant	Etchant	Etchant capping agent	Etchant	Etchant
Br ⁻	—	Etchant capping agent	—	Etchant capping agent	Etchant
I ⁻	—	—	—	Etchant capping agent	—
O ₂	Etchant	Etchant	Etchant	Etchant	Etchant
H ₂ O ₂	Etchant	—	—	—	—
Fe(III)/Fe(II)	Protection in EG; etchant in oleylamine	Etchant	—	Etchant	—
Cu(II)/Cu(I)	Protection	Etchant	—	—	—
TOP	—	—	Etchant	—	—
CN ⁻	—	Etchant	—	—	—
Citric acid	—	Protection	—	Protection	—
Inert gas	Protection	Protection	Protection	Protection	—

an impurity in solvents. As previously mentioned, due to the fact that these etchants are often present during synthesis, both the product homogeneity and synthesis reproducibility have been dramatically improved since the discovery of this etchant pair.

The strength of oxidative etching is a critical parameter to how significantly the etching may impact a synthesis. The common way to enhance oxidative etching is the combination of multiple components. As demonstrated in Table 5, the etching strength of Cl⁻ and O₂ can be greatly increased by addition of acid; halide ions may act as a ligand to reduce the potentials of metals, which facilitates the etching of metal nanocrystals by oxidative etchants such as Fe(III). From this table, it is also well recognized that the potentials of species are highly dependent on environmental factors such as pH value and ligand complexation, which essentially can be understood from the Nernst Equation.

The simplest way to prevent oxidative etching is the protection of reactions under the flow of inert gas such as N₂ and Ar. This fact suggests that oxygen is the major cause of etching in most systems. For the case of Cl⁻ and O₂, oxygen plays the

central role in oxidation while chloride is mainly responsible for corrosion and potential reduction. Without the assistance of oxygen, halide ions cannot etch metal structures. In certain cases such as Pd, it is not feasible to completely eliminate the oxygen in reactions by bubbling inert gas. For this reason, protection agents such as citric acid have been developed to remove the oxygen from the system. To achieve tunable oxidative etching, more protection agents should be screened and developed in the future.

3. Properties of metal nanocrystals tuned by oxidation etching

The morphologies and surface structures of metal nanocrystals have a huge impact on their chemical and physical properties. Oxidative etching provides a knob to tune the physical parameters of metal nanocrystals so as to optimize their properties for various applications. In this section, we highlight a few examples for tunable catalytic and optical properties, based on the nanocrystals whose parameters are tailored *via* oxidative etching.

In terms of catalysis, high-index facets generally exhibit higher catalytic activities than low-index ones, because they have a greater percentage of unsaturated atomic steps, edges, and kinks which can serve as intrinsically more active sites for catalysis. As demonstrated in Section 2.2.2, the Pd concave structures prepared by the etching activation can maintain the particle size comparable to that of their seeds. The selective site activation by oxidative etching offers the possibility to achieve highly controllable epitaxial growth on metal nanocrystals without atomic addition on undesired locations. The high-index surfaces allow this structure to exhibit superior catalytic performance. In formic acid oxidation, the maximum current densities by the size-maintained concave nanocubes are twofold and fivefold higher than those by concave structures in the literature and nanocubes, respectively. When a limited amount of Pt (only 3.3 wt%) is selectively deposited on Pd nanocubes, the Pd–Pt nanocubes exhibit an activity of 4.7 mA cm⁻², which is 2.5 times and 1.9 times greater than those of Pd nanocubes and Pt/C commercial catalysts, respectively (Fig. 14a and b).⁷⁶ From the discussion here, it can be concluded that maximization of surface atoms (particularly on edges and corners) should be

Table 5 Standard potentials of redox pairs involved in oxidative etching⁷⁰

Half reaction	<i>E</i> ⁰
Ag ⁺ + e ⁻ → Ag	0.7996
AgBr + e ⁻ → Ag + Br ⁻	0.07133
AgCl + e ⁻ → Ag + Cl ⁻	0.22233
Ag ₂ SO ₄ + e ⁻ → 2Ag + SO ₄ ²⁻	0.654
Au ³⁺ + 2e ⁻ → Au ⁺	1.36
Au ⁺ + e ⁻ → Au	1.83
Au ³⁺ + 3e ⁻ → Au	1.52
AuBr ₄ ⁻ + 3e ⁻ → Au + 4Br ⁻	0.854
AuCl ₄ ⁻ + 3e ⁻ → Au + 4Cl ⁻	1.002
Pd ²⁺ + 2e ⁻ → Pd	0.915
PdBr ₄ ²⁻ + 2e ⁻ → Pd + 4Br ⁻	0.49
PdCl ₄ ²⁻ + 2e ⁻ → Pd + 4Cl ⁻	0.591
Pt ²⁺ + 2e ⁻ → Pt	1.188
PtCl ₄ ²⁻ + 2e ⁻ → Pt + 4Cl ⁻	0.755
Rh ³⁺ + 3e ⁻ → Rh	0.758
Fe ³⁺ + e ⁻ → Fe ²⁺	0.771
Fe ²⁺ + 2e ⁻ → Fe	-0.447
Fe ³⁺ + 3e ⁻ → Fe	-0.037
Cu ⁺ + e ⁻ → Cu	0.521
Cu ²⁺ + e ⁻ → Cu ⁺	0.153
Ni ²⁺ + 2e ⁻ → Ni	-0.257
O ₂ + 4H ⁺ + 4e ⁻ → 2H ₂ O	1.229
O ₂ + 2H ₂ O + 4e ⁻ → 4OH ⁻	0.401
H ₂ O ₂ + 2e ⁻ → 2OH ⁻	0.867
H ₂ O ₂ + 2H ⁺ + 2e ⁻ → 2H ₂ O	1.763

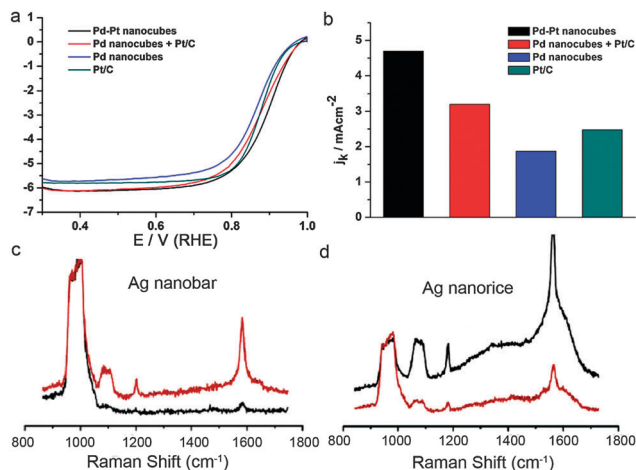


Fig. 14 (a) ORR polarization curves for Pd–Pt nanocubes, Pd nanocubes, Pt/C and mixed reference samples in an O₂-saturated 0.1 M HClO₄ solution with a sweep rate of 20 mV s⁻¹. (b) Kinetic current densities (j_k) at 0.9 V versus RHE for the four samples normalized by the geometric area of electrodes (adapted with permission from ref. 76, Copyright 2013 Royal Society of Chemistry). SERS spectra of (c) a single nanobar and (d) a single nanorice covered by a 1,4-benzenedithiol monolayer (red: transverse polarization; black: longitudinal polarization) (adapted with permission from ref. 88, Copyright 2007 American Chemical Society).

the criteria for the design of metal nanocrystals. To fulfil such a design, oxidative etching is a convenient tool that can facilitate the formation of high-index facets. Without the need for introducing additional capping agents, the shape and structural control by etching can keep the surface chemistry of all the samples relatively identical. As such, it becomes feasible to reliably evaluate the shape- and structure-dependent catalytic performance without much concern on the interference from varied ligands.

Another important property of noble metals is LSPR: under the irradiation of light, the alternating electric field can drive the free electrons in metals to collectively oscillate in phase with incident light.¹⁰⁹ This near-field effect can enhance the Raman scattering cross sections of molecules adsorbed on a nanoparticle surface. This effect, known as the SERS, is a useful technique for molecular sensing, especially for the detection of low-concentration analytes.^{110–115} Shape control of coinage metals brought about by oxidative etching can manipulate the LSPR features in a spectrum, resulting in a diversification of SERS substrate materials. Corners- and edges-etched nanoparticles have different polarizations compared with unetched nanoparticles (Fig. 14c and d). Thus shape control of metal nanoparticles brought about by oxidative etching can expand the scope of sensing applications.

Certainly there are some other applications based on the metal nanocrystals whose synthesis requires tightly tuning the parameter of oxidative etching. For instance, metal nanowires should be synthesized by blocking the effect of oxidative etching on twin seed removal, and have shown promising applications in plasmonic waveguiding and flexible electronics.^{22,116–123} Overall, the deliberate synthesis enabled by the oxidative etching opens a window to produce nanostructures with various desired parameters and functions.

4. Potential extension of oxidative etching to other materials and hybrid structures

As a matter of fact, the oxidative etching has been utilized in the synthesis of carbon as well as semiconductors. Taking single-walled carbon nanotubes for example, piranha solution (4 : 1 vol/vol: 96% H₂SO₄/30% H₂O₂) is capable of attacking existing damaged sites in the nanotube sidewall and cutting the nanotubes.¹²⁴ In the semiconductor field, oxidative etching has broader applications. Nie *et al.* reported an oxidative mechanism involving HOCl and H₂O₂ that can diffuse across the polymer coating layer causing surface oxidation of quantum dots. This oxidative etching process generates lattice defects and quenches fluorescence.¹²⁵ Yang *et al.* produced jagged Cu₂O polyhedra covered with numerous {110} edges and {111} corners by using sodium citrate and dehydroascorbic acid to etch the {111} facets of octahedra.¹²⁶ Lee *et al.* reported hollow Mn-doped Fe₃O₄ nanostructures by etching the MnO from MnO–Fe₃O₄ core-shell structures.¹²⁷

Interestingly, silicon nanowire arrays can be fabricated *via* a metal-assisted etching process.^{128–131} Ag and Au are the metals commonly used in this approach, while Pt, Pd, Cu and Ni have also been extensively studied.^{132–138} During the etching process, metal nanoparticles behave like a cathode, and surrounding Si area works as an anode which is etched down by HF. More specifically, the redox reaction process occurs with the HF etching as follows: $M^{n+} + ne^- = M^0$; $Si^0 + 6F^- = SiF_6^{2-} + 4e^-$. The diameter, length and density of Si nanowire arrays can be readily controlled by adjusting the parameters of metals and Si wafers. Such Si nanowire arrays have found their use in photovoltaics,^{139,140} photocatalysis^{141,142} and photodetectors.¹⁴³

It is expected that oxidative etching can be extended to the design of metal–semiconductor hybrid structures that have wide applications in photocatalysis and optoelectronics.^{144–146} Most recently, this strategy was achieved on Cu₂O to form well-designed metal–semiconductor hybrid structures.^{147–149} When experimental parameters are well controlled, certain surfaces of Cu₂O can be etched by noble metal salts such as AuCl₄⁻ or PdCl₄²⁻ *via* redox reactions ($nCu_2O + 2M^{n+} + 2nH^+ \rightarrow 2M + 2nCu^{2+} + nH_2O$). As a result, the reduced Au or Pd atoms can selectively grow on the Cu₂O nanocrystal surface to form metal–Cu₂O hybrid structures which have shown improved photocatalytic performance. It is anticipated that more efforts could be made on the fabrication of metal–semiconductor hybrid structures by taking advantage of oxidative etching once the growth site activation is more controllable.

5. Conclusions and outlook

In this review, we have outlined recent progress in the functions of oxidative etching in direct synthesis and post-synthesis reshaping, with a focus on the fundamentals behind each synthesis and process. Atomic addition and subtraction are part of all the evolutions between atoms, clusters and nanocrystals driven by

oxidative etching, and as such, the etching approach represents an atomic-level control over the physical parameters of metal nanocrystals. There has been a surge of research activities on metal nanocrystals for various applications in the last decade, a few of which have been highlighted as examples to show the impact of oxidative etching in the research fields. For the space limit, it seems not very feasible to include all the reported cases in this review article. Nevertheless, it is well established that the performance of metal nanocrystals is ultimately determined by its intrinsic parameters. Thus it is believed that the tool of oxidative etching will be continuously employed by the community to significantly improve the controllability of nanocrystals synthesis when the reaction environment and pathways are tightly controlled.

Despite the success in the use of oxidative etching, there still remain lots of challenges and opportunities for further development of oxidative etching for nanocrystals synthesis. The first challenge comes from the complexity induced by etchant species. For instance, bromide as a well-demonstrated etchant may have multiple functions that are interlinked together: capping on {100} facets to maneuver surface facets, and formation of complex ions (e.g., $[\text{PdBr}_4]^{2-}$) or precipitates (e.g., AgBr) to alter reaction kinetics. This feature would constitute a major limitation on the controllability of oxidative etching. Thus it is imperative to develop a library of new etchants, in which some ideas of etching in semiconductor-processing techniques may be borrowed. It is anticipated that this development will boost the applications of oxidative etching in the near future.

Second, no anisotropic etching has yet been demonstrated in the synthesis of metal nanocrystals, although it has capabilities to control the crystallinity of seeds (single-crystal *versus* twinned). Certainly fcc is a structure with high symmetry, so it may be more difficult to develop anisotropic etching like the silicon system despite few reports on Cu.^{150,151} However, enlightened by the pitting mode, we envision that it would be feasible to develop some approaches to anisotropic etching combined with capping methods. As long as one or a few faces of nanocrystals can be selectively functionalized by capping agents,¹⁵² oxidative etching will preferentially occur on the other faces to induce anisotropic etching.

Certainly, these challenges indicate that lots of opportunities are around the corner for the research community. For instance, the combination of oxidative etching with capping agents will enable highly controllable atomic subtraction to carve the nanocrystals and make new surface facets or hollow structures (which have been demonstrated in some cases) as well as atomic addition on activated sites to grow anisotropic structures or form high-index facets.

Finally, we would like to mention that the applications of oxidative etching are not limited to the metal nanocrystals. Similar to the strategy for making metal materials, certain locations on metal nanocrystals can be selectively activated by etching to provide growth sites for semiconductors (or *vice versa*), formulating well-designed metal–semiconductor hybrid structures. Research along these lines will turn oxidative etching into a more powerful and versatile tool in the fields of materials science and nanoscience.

Acknowledgements

This work was financially supported by the 973 Program (No. 2014CB848900), the National Natural Science Foundation of China (NSFC) (No. 21101145, 91123010), the Recruitment Program of Global Experts, the CAS Hundred Talent Program, and the Fundamental Research Funds for the Central Universities (No. WK2060190025, WK2060190037).

Notes and references

- 1 Y. Xia, Y. Xiong, B. Lim and S. E. Skrabalak, *Angew. Chem., Int. Ed.*, 2009, **48**, 60–103.
- 2 D. J. Smith, A. K. Petfordlong, L. R. Wallenberg and J. O. Bovin, *Science*, 1986, **233**, 872–875.
- 3 H. H. Huang, X. P. Ni, G. L. Loy, C. H. Chew, K. L. Tan, F. C. Loh, J. F. Deng and G. Q. Xu, *Langmuir*, 1996, **12**, 909–912.
- 4 T. S. Ahmadi, Z. L. Wang, A. Henglein and M. A. ElSayed, *Chem. Mater.*, 1996, **8**, 1161–1163.
- 5 J. C. Weeber, A. Dereux, C. Girard, J. R. Krenn and J. P. Goudonnet, *Phys. Rev. B: Condens. Matter Mater. Phys.*, 1999, **60**, 9061–9068.
- 6 S. H. Sun, C. B. Murray, D. Weller, L. Folks and A. Moser, *Science*, 2000, **287**, 1989–1992.
- 7 R. C. Jin, S. Egusa and N. F. Scherer, *J. Am. Chem. Soc.*, 2004, **126**, 9900–9901.
- 8 F. S. Han, *Chem. Soc. Rev.*, 2013, **42**, 5270–5298.
- 9 H. J. You, S. C. Yang, B. J. Ding and H. Yang, *Chem. Soc. Rev.*, 2013, **42**, 2880–2904.
- 10 T. G. Kelly and J. G. Chen, *Chem. Soc. Rev.*, 2012, **41**, 8021–8034.
- 11 B. Hvolbaek, T. V. W. Janssens, B. S. Clausen, H. Falsig, C. H. Christensen and J. K. Nørskov, *Nano Today*, 2007, **2**, 14–18.
- 12 R. Franzen, *Can. J. Chem.*, 2000, **78**, 957–962.
- 13 S. W. Kim, M. Kim, W. Y. Lee and T. Hyeon, *J. Am. Chem. Soc.*, 2002, **124**, 7642–7643.
- 14 C. Wang, L. Ma, L. Liao, S. Bai, R. Long, M. Zuo and Y. Xiong, *Sci. Rep.*, 2013, **3**, 2580.
- 15 B. K. Jena and C. R. Raj, *Langmuir*, 2007, **23**, 4064–4070.
- 16 M. Jin, H. Liu, H. Zhang, Z. Xie, J. Liu and Y. Xia, *Nano Res.*, 2010, **4**, 83–91.
- 17 M. P. Cecchini, V. A. Turek, J. Paget, A. A. Kornyshev and J. B. Edl, *Nat. Mater.*, 2013, **12**, 165–171.
- 18 M. J. Mulvihill, X. Y. Ling, J. Henzie and P. Yang, *J. Am. Chem. Soc.*, 2010, **132**, 268–274.
- 19 Y. Xiong, J. M. McLellan, J. Chen, Y. Yin, Z. Y. Li and Y. Xia, *J. Am. Chem. Soc.*, 2005, **127**, 17118–17127.
- 20 J. M. McLellan, Z.-Y. Li, A. R. Siekkinen and Y. Xia, *Nano Lett.*, 2007, **7**, 1013–1017.
- 21 S. Jeong, K. Woo, D. Kim, S. Lim, J. S. Kim, H. Shin, Y. Xia and J. Moon, *Adv. Funct. Mater.*, 2008, **18**, 679–686.
- 22 L. Hu, H. S. Kim, J. Y. Lee, P. Peumans and Y. Cui, *ACS Nano*, 2010, **4**, 2955–2963.

- 23 P. K. Khanna, N. Singh, S. Charan, V. V. V. S. Subbarao, R. Gokhale and U. P. Mulik, *Mater. Chem. Phys.*, 2005, **93**, 117–121.
- 24 A. R. Madaria, A. Kumar, F. N. Ishikawa and C. Zhou, *Nano Res.*, 2010, **3**, 564–573.
- 25 M. Gericke and A. Pinches, *Hydrometallurgy*, 2006, **83**, 132–140.
- 26 J. L. West and N. J. Halas, *Annu. Rev. Biomed. Eng.*, 2003, **5**, 285–292.
- 27 M. S. Shim and Y. Xia, *Angew. Chem., Int. Ed.*, 2013, **52**, 6926–6929.
- 28 R. R. Arvizo, S. Bhattacharyya, R. A. Kudgus, K. Giri, R. Bhattacharya and P. Mukherjee, *Chem. Soc. Rev.*, 2012, **41**, 2943–2970.
- 29 Y. J. Xiong, A. R. Siekkinen, J. G. Wang, Y. D. Yin, M. J. Kim and Y. N. Xia, *J. Mater. Chem.*, 2007, **17**, 2600–2602.
- 30 Y. Ma, W. Li, J. Zeng, M. McKiernan, Z. Xie and Y. Xia, *J. Mater. Chem.*, 2010, **20**, 3586–3589.
- 31 Y. J. Xiong, *Chem. Commun.*, 2011, **47**, 1580–1582.
- 32 Y. Xiong, H. Cai, B. J. Wiley, J. Wang, M. J. Kim and Y. Xia, *J. Am. Chem. Soc.*, 2007, **129**, 3665–3675.
- 33 Y. Wang, S. Xie, J. Liu, J. Park, C. Z. Huang and Y. Xia, *Nano Lett.*, 2013, **13**, 2276–2281.
- 34 C. M. Wang, L. L. Wang, R. Long, L. Ma, L. M. Wang, Z. Q. Li and Y. J. Xiong, *J. Mater. Chem.*, 2012, **22**, 8195–8198.
- 35 Q. X. Guo, Y. S. Zhao, W. L. Mao, Z. W. Wang, Y. J. Xiong and Y. N. Xia, *Nano Lett.*, 2008, **8**, 972–975.
- 36 Y. Xiong, I. Washio, J. Chen, M. Sadilek and Y. N. Xia, *Angew. Chem., Int. Ed.*, 2007, **46**, 4917–4921.
- 37 M. Tsuji, N. Miyamae, M. Nishio, S. Hikino and N. Ishigami, *Bull. Chem. Soc. Jpn.*, 2007, **80**, 2024–2038.
- 38 S. Maksimuk, X. Teng and H. Yang, *Phys. Chem. Chem. Phys.*, 2006, **8**, 4660–4663.
- 39 J. S. Spendelow and A. Wieckowski, *Phys. Chem. Chem. Phys.*, 2004, **6**, 5094–5118.
- 40 T. A. Land, T. L. Martin, S. Potapenko, G. T. Palmore and J. J. De Yoreo, *Nature*, 1999, **399**, 442–445.
- 41 C. T. Campbell, *Surf. Sci.*, 1985, **157**, 43–60.
- 42 K. Habermehl-Cwirzen and J. Lahtinen, *Surf. Sci.*, 2004, **573**, 183–190.
- 43 M. W. Roberts, *Surf. Sci.*, 1994, **299**, 769–784.
- 44 E. H. Voogt, A. J. M. Mens, O. L. J. Gijzeman and J. W. Geus, *Surf. Sci.*, 1997, **373**, 210–220.
- 45 Z. L. Wang, M. B. Mohamed, S. Link and M. A. El-Sayed, *Surf. Sci.*, 1999, **440**, L809–L814.
- 46 Y. Xiong and Y. Xia, *Adv. Mater.*, 2007, **19**, 3385–3391.
- 47 B. Wiley, T. Herricks, Y. G. Sun and Y. N. Xia, *Nano Lett.*, 2004, **4**, 1733–1739.
- 48 Y. Xiong, J. Chen, B. Wiley, Y. Xia, S. Aloni and Y. Yin, *J. Am. Chem. Soc.*, 2005, **127**, 7332–7333.
- 49 L. Ma, C. Wang, M. Gong, L. Liao, R. Long, J. Wang, D. Wu, W. Zhong, M. J. Kim, Y. Chen, Y. Xie and Y. Xiong, *ACS Nano*, 2012, **6**, 9797–9806.
- 50 A. I. Hochbaum, R. K. Chen, R. D. Delgado, W. J. Liang, E. C. Garnett, M. Najarian, A. Majumdar and P. D. Yang, *Nature*, 2008, **451**, 163–165.
- 51 C. M. Cobley, M. Rycenga, F. Zhou, Z. Y. Li and Y. Xia, *Angew. Chem., Int. Ed.*, 2009, **48**, 4824–4827.
- 52 X. Guo, Q. Zhang, Y. Sun, Q. Zhao and J. Yang, *ACS Nano*, 2012, **6**, 1165–1175.
- 53 C. C. Huang, J. R. Hwu, W. C. Su, D. B. Shieh, Y. Tzeng and C. S. Yeh, *Chem. – Eur. J.*, 2006, **12**, 3805–3810.
- 54 A. Kisner, M. Heggen, E. Fernandez, S. Lenk, D. Mayer, U. Simon, A. Offenhauser and Y. Mourzina, *Chem. – Eur. J.*, 2011, **17**, 9503–9507.
- 55 X. Xia, S. I. Choi, J. A. Herron, N. Lu, J. Scaranto, H. C. Peng, J. Wang, M. Mavrikakis, M. J. Kim and Y. Xia, *J. Am. Chem. Soc.*, 2013, **135**, 15706–15709.
- 56 S. Xie, N. Lu, Z. Xie, J. Wang, M. J. Kim and Y. Xia, *Angew. Chem., Int. Ed.*, 2012, **51**, 10266–10270.
- 57 H. Zhang, X. Xia, W. Li, J. Zeng, Y. Dai, D. Yang and Y. Xia, *Angew. Chem., Int. Ed.*, 2010, **49**, 5296–5300.
- 58 Y. Xiong, R. Long, D. Liu, X. Zhong, C. Wang, Z. Y. Li and Y. Xie, *Nanoscale*, 2012, **4**, 4416–4420.
- 59 S. Diez-Gonzalez, N. Marion and S. P. Nolan, *Chem. Rev.*, 2009, **109**, 3612–3676.
- 60 B. Wiley, T. Herricks, Y. Sun and Y. Xia, *Nano Lett.*, 2004, **4**, 1733–1739.
- 61 F. Baletto and R. Ferrando, *Rev. Mod. Phys.*, 2005, **77**, 371–423.
- 62 S. H. Im, Y. T. Lee, B. Wiley and Y. Xia, *Angew. Chem., Int. Ed.*, 2005, **117**, 2192–2195.
- 63 B. Wiley, Y. Sun and Y. Xia, *Langmuir*, 2005, **21**, 8077–8080.
- 64 A. Tao, P. Sinsermsuksakul and P. Yang, *Angew. Chem., Int. Ed.*, 2006, **45**, 4597–4601.
- 65 Q. A. Zhang, W. Y. Li, C. Moran, J. Zeng, J. Y. Chen, L. P. Wen and Y. N. Xia, *J. Am. Chem. Soc.*, 2010, **132**, 11372–11378.
- 66 B. Li, R. Long, X. Zhong, Y. Bai, Z. Zhu, X. Zhang, M. Zhi, J. He, C. Wang, Z. Y. Li and Y. Xiong, *Small*, 2012, **8**, 1710–1716.
- 67 Y. Wang, Y. Zheng, C. Z. Huang and Y. Xia, *J. Am. Chem. Soc.*, 2013, **135**, 1941–1951.
- 68 K. E. Korte, S. E. Skrabalak and Y. Xia, *J. Mater. Chem.*, 2008, **18**, 437–441.
- 69 B. J. Wiley, Y. Xiong, Z. Y. Li, Y. Yin and Y. Xia, *Nano Lett.*, 2006, **6**, 765–768.
- 70 R. L. David and W. M. Haynes, *CRC Handbook of Chemistry and Physics*, 90th edn, 2010.
- 71 S. E. Skrabalak, B. J. Wiley, M. Kim, E. V. Formo and Y. Xia, *Nano Lett.*, 2008, **8**, 2077–2081.
- 72 C. Wang, S. Peng, R. Chan and S. Sun, *Small*, 2009, **5**, 567–570.
- 73 R. Chinchilla and C. Najera, *Chem. Rev.*, 2013, **114**, 1783–1826.
- 74 M. Crespo-Quesada, A. Yarulin, M. Jin, Y. Xia and L. Kiwi-Minsker, *J. Am. Chem. Soc.*, 2011, **133**, 12787–12794.
- 75 R. Long, K. Mao, X. Ye, W. Yan, Y. Huang, J. Wang, Y. Fu, X. Wang, X. Wu, Y. Xie and Y. Xiong, *J. Am. Chem. Soc.*, 2013, **135**, 3200–3207.
- 76 Y. Bai, R. Long, C. Wang, M. Gong, Y. Li, H. Huang, H. Xu, Z. Li, M. Deng and Y. Xiong, *J. Mater. Chem. A*, 2013, **1**, 4228–4235.

- 77 Y. J. Xiong, J. M. McLellan, Y. D. Yin and Y. N. Xia, *Angew. Chem., Int. Ed.*, 2007, **46**, 790–794.
- 78 S. Eustis and M. A. El-Sayed, *Chem. Soc. Rev.*, 2006, **35**, 209–217.
- 79 C. M. Cobley, J. Y. Chen, E. C. Cho, L. V. Wang and Y. N. Xia, *Chem. Soc. Rev.*, 2011, **40**, 44–56.
- 80 E. Boisselier and D. Astruc, *Chem. Soc. Rev.*, 2009, **38**, 1759–1782.
- 81 W. Li and Y. Xia, *Chem. – Asian J.*, 2010, **5**, 1312–1316.
- 82 D. Seo, C. Il Yoo, I. S. Chung, S. M. Park, S. Ryu and H. Song, *J. Phys. Chem. C*, 2008, **112**, 2469–2475.
- 83 Z. Li, J. Tao, X. Lu, Y. Zhu and Y. Xia, *Nano Lett.*, 2008, **8**, 3052–3055.
- 84 Z. R. Guo, Y. Zhang, A. Q. Xu, M. Wang, L. Huang, K. Xu and N. Gu, *J. Phys. Chem. C*, 2008, **112**, 12638–12645.
- 85 X. Lu, M. S. Yavuz, H. Y. Tuan, B. A. Korgel and Y. Xia, *J. Am. Chem. Soc.*, 2008, **130**, 8900–8901.
- 86 M. Jin, G. He, H. Zhang, J. Zeng, Z. Xie and Y. Xia, *Angew. Chem., Int. Ed.*, 2011, **50**, 10560–10564.
- 87 H. Guo, Y. Chen, H. Ping, J. Jin and D. L. Peng, *Nanoscale*, 2013, **5**, 2394–2402.
- 88 B. J. Wiley, Y. Chen, J. M. McLellan, Y. Xiong, Z. Y. Li, D. Ginger and Y. Xia, *Nano Lett.*, 2007, **7**, 1032–1036.
- 89 Q. Zhang, N. Li, J. Goebel, Z. Lu and Y. Yin, *J. Am. Chem. Soc.*, 2011, **133**, 18931–18939.
- 90 B. J. Wiley, S. H. Im, Z. Y. Li, J. McLellan, A. Siekkinen and Y. Xia, *J. Phys. Chem. B*, 2006, **110**, 15666–15675.
- 91 Q. Zhang, W. Li, L. P. Wen, J. Chen and Y. Xia, *Chem. – Eur. J.*, 2010, **16**, 10234–10239.
- 92 Y. Xiong, J. Chen, B. Wiley, Y. Xia, Y. Yin and Z. Y. Li, *Nano Lett.*, 2005, **5**, 1237–1242.
- 93 S. H. Zhang, Z. Y. Jiang, Z. X. Xie, X. Xu, R. B. Huang and L. S. Zheng, *J. Phys. Chem. B*, 2005, **109**, 9416–9421.
- 94 R. C. Newman and K. Sieradzki, *Science*, 1994, **263**, 1708–1709.
- 95 H. Guo, Y. Chen, H. Ping, L. Wang and D.-L. Peng, *J. Mater. Chem.*, 2012, **22**, 8336–8344.
- 96 I. R. Harris, I. L. Dillamore, R. E. Smallman and B. E. P. Beeston, *Philos. Mag.*, 1966, **14**, 325–333.
- 97 S. Kibey, J. B. Liu, D. D. Johnson and H. Sehitoglu, *Acta Mater.*, 2007, **55**, 6843–6851.
- 98 J. W. Mullin, *Crystallization*, Butterworth-Heinemann, London, 1961.
- 99 A. Roucoux, J. Schulz and H. Patin, *Chem. Rev.*, 2002, **102**, 3757–3778.
- 100 G. Boisvert, L. J. Lewis and M. Scheffler, *Phys. Rev. B: Condens. Matter Mater. Phys.*, 1998, **57**, 1881–1889.
- 101 Y. Xiong, B. Wiley, J. Chen, Z. Y. Li, Y. Yin and Y. Xia, *Angew. Chem., Int. Ed.*, 2005, **44**, 7913–7917.
- 102 C. M. Cobley, M. Rycenga, F. Zhou, Z. Y. Li and Y. N. Xia, *J. Phys. Chem. C*, 2009, **113**, 16975–16982.
- 103 J. Xu, S. Li, J. Weng, X. Wang, Z. Zhou, K. Yang, M. Liu, X. Chen, Q. Cui, M. Cao and Q. Zhang, *Adv. Funct. Mater.*, 2008, **18**, 277–284.
- 104 R. Zou, X. Guo, J. Yang, D. Li, F. Peng, L. Zhang, H. Wang and H. Yu, *CrystEngComm*, 2009, **11**, 2797.
- 105 C. K. Tsung, X. Kou, Q. Shi, J. Zhang, M. H. Yeung, J. Wang and G. D. Stucky, *J. Am. Chem. Soc.*, 2006, **128**, 5352–5353.
- 106 T. S. Sreeprasad, A. K. Samal and T. Pradeep, *Langmuir*, 2007, **23**, 9463–9471.
- 107 M. Liu, Y. Zheng, L. Zhang, L. Guo and Y. Xia, *J. Am. Chem. Soc.*, 2013, **135**, 11752–11755.
- 108 M. Jin, H. Zhang, Z. Xie and Y. Xia, *Angew. Chem., Int. Ed.*, 2011, **50**, 7850–7854.
- 109 Y. N. Xia and N. J. Halas, *MRS Bull.*, 2005, **30**, 338–344.
- 110 H. A. Atwater and A. Polman, *Nat. Mater.*, 2010, **9**, 205–213.
- 111 C. L. Haynes, A. D. McFarland and R. P. Van Duyne, *Anal. Chem.*, 2005, **77**, 338A–346A.
- 112 Y. J. Xiong, R. Long, D. Liu, X. L. Zhong, C. M. Wang, Z. Y. Li and Y. Xie, *Nanoscale*, 2012, **4**, 4416–4420.
- 113 A. J. Haes, C. L. Haynes, A. D. McFarland, G. C. Schatz, R. R. Van Duyne and S. L. Zou, *MRS Bull.*, 2005, **30**, 368–375.
- 114 G. Baffou, R. Quidant and C. Girard, *Appl. Phys. Lett.*, 2009, **94**, 153109.
- 115 C. W. Chang, D. Okawa, A. Majumdar and A. Zettl, *Science*, 2006, **314**, 1121–1124.
- 116 R. M. Mutiso, M. C. Sherrott, A. R. Rathmell, B. J. Wiley and K. I. Winey, *ACS Nano*, 2013, **7**, 7654–7663.
- 117 A. W. Sanders, D. A. Routenberg, B. J. Wiley, Y. Xia, E. R. Dufresne and M. A. Reed, *Nano Lett.*, 2006, **6**, 1822–1826.
- 118 A. L. Pyayt, B. Wiley, Y. N. Xia, A. Chen and L. Dalton, *Nat. Nanotechnol.*, 2008, **3**, 660–665.
- 119 M. Ohtsu, K. Kobayashi, T. Kawazoe, S. Sangu and T. Yatsui, *IEEE J. Sel. Top. Quantum Electron.*, 2002, **8**, 839–862.
- 120 T. Yatsui, M. Kourogi and M. Ohtsu, *Appl. Phys. Lett.*, 2001, **79**, 4583–4585.
- 121 J. Wu, J. Zang, A. R. Rathmell, X. Zhao and B. J. Wiley, *Nano Lett.*, 2013, **13**, 2381–2386.
- 122 A. R. Rathmell and B. J. Wiley, *Adv. Mater.*, 2011, **23**, 4798–4803.
- 123 S. M. Bergin, Y. H. Chen, A. R. Rathmell, P. Charbonneau, Z. Y. Li and B. J. Wiley, *Nanoscale*, 2012, **4**, 1996–2004.
- 124 K. J. Ziegler, Z. Gu, H. Peng, E. L. Flor, R. H. Hauge and R. E. Smalley, *J. Am. Chem. Soc.*, 2005, **127**, 1541–1547.
- 125 M. C. Mancini, B. A. Kairdolf, A. M. Smith and S. M. Nie, *J. Am. Chem. Soc.*, 2008, **130**, 10836–10837.
- 126 Y. Shang, D. Sun, Y. Shao, D. Zhang, L. Guo and S. Yang, *Chem. – Eur. J.*, 2012, **18**, 14261–14266.
- 127 V. N. Phan, E. K. Lim, T. Kim, M. Kim, Y. Choi, B. Kim, M. Lee, A. Oh, J. Jin, Y. Chae, H. Baik, J. S. Suh, S. Haam, Y. M. Huh and K. Lee, *Adv. Mater.*, 2013, **25**, 3202–3208.
- 128 Z. Huang, H. Fang and J. Zhu, *Adv. Mater.*, 2007, **19**, 744–748.
- 129 K. Q. Peng, Y. J. Yan, S. P. Gao and J. Zhu, *Adv. Mater.*, 2002, **14**, 1164–1167.
- 130 Z. Huang, X. Zhang, M. Reiche, L. Liu, W. Lee, T. Shimizu, S. Senz and U. Gosele, *Nano Lett.*, 2008, **8**, 3046–3051.
- 131 W. K. Choi, T. H. Liew, M. K. Dawood, H. I. Smith, C. V. Thompson and M. H. Hong, *Nano Lett.*, 2008, **8**, 3799–3802.

- 132 P. Gorostiza, R. Diaz, J. Servat, F. Sanz and J. R. Morante, *J. Electrochem. Soc.*, 1997, **144**, 909–914.
- 133 P. Gorostiza, M. A. Kulandainathan, R. Diaz, F. Sanz, P. Allongue and J. R. Morante, *J. Electrochem. Soc.*, 2000, **147**, 1026–1030.
- 134 G. V. Kuznetsov, V. A. Skryshevsky, T. A. Vdovenkova, A. I. Tsyganova, P. Gorostiza and F. G. Sanz, *J. Electrochem. Soc.*, 2001, **148**, C528–C532.
- 135 L. A. Nagahara, T. Ohmori, K. Hashimoto and A. Fujishima, *J. Vac. Sci. Technol., A*, 1993, **11**, 763–767.
- 136 K. Q. Peng, Y. Wu, H. Fang, X. Y. Zhong, Y. Xu and J. Zhu, *Angew. Chem., Int. Ed.*, 2005, **44**, 2737–2742.
- 137 K. Q. Peng, H. Fang, J. J. Hu, Y. Wu, J. Zhu, Y. J. Yan and S. Lee, *Chem. – Eur. J.*, 2006, **12**, 7942–7947.
- 138 K. Q. Peng, A. J. Lu, R. Q. Zhang and S. T. Lee, *Adv. Funct. Mater.*, 2008, **18**, 3026–3035.
- 139 K. Q. Peng, Y. Xu, Y. Wu, Y. J. Yan, S. T. Lee and J. Zhu, *Small*, 2005, **1**, 1062–1067.
- 140 C. Xie, P. Lv, B. A. Nie, J. S. Jie, X. W. Zhang, Z. Wang, P. Jiang, Z. Z. Hu, L. B. Luo, Z. F. Zhu, L. Wang and C. Y. Wu, *Appl. Phys. Lett.*, 2011, **99**, 133113.
- 141 M. W. Shao, L. Cheng, X. H. Zhang, D. D. D. Ma and S. T. Lee, *J. Am. Chem. Soc.*, 2009, **131**, 17738–17739.
- 142 F. Y. Wang, Q. D. Yang, G. Xu, N. Y. Lei, Y. K. Tsang, N. B. Wong and J. C. Ho, *Nanoscale*, 2011, **3**, 3269–3276.
- 143 C. Xie, B. Nie, L. Zeng, F.-X. Liang, M.-Z. Wang, L. Luo, M. Feng, Y. Yu, C.-Y. Wu, Y. Wu and S.-H. Yu, *ACS Nano*, 2014, 4015–4022.
- 144 K. C. F. Leung, S. H. Xuan, X. M. Zhu, D. W. Wang, C. P. Chak, S. F. Lee, W. K. W. Ho and B. C. T. Chung, *Chem. Soc. Rev.*, 2012, **41**, 1911–1928.
- 145 H. L. Wang and H. J. Dai, *Chem. Soc. Rev.*, 2013, **42**, 3088–3113.
- 146 H. J. Chen, L. Shao, Q. Li and J. F. Wang, *Chem. Soc. Rev.*, 2013, **42**, 2679–2724.
- 147 X. W. Liu, *Langmuir*, 2011, **27**, 9100–9104.
- 148 E. M. Zahran, N. M. Bedford, M. A. Nguyen, Y. J. Chang, B. S. Guiton, R. R. Naik, L. G. Bachas and M. R. Knecht, *J. Am. Chem. Soc.*, 2014, **136**, 32–35.
- 149 L. Wang, J. Ge, A. Wang, M. Deng, X. Wang, S. Bai, R. Li, J. Jiang, Q. Zhang, Y. Luo and Y. Xiong, *Angew. Chem., Int. Ed.*, 2014, **53**, 5107–5111.
- 150 W. X. Niu, Z. Y. Li, L. H. Shi, X. Q. Liu, H. J. Li, S. Han, J. Chen and G. B. Xu, *Cryst. Growth Des.*, 2008, **8**, 4440–4444.
- 151 D. Vogel, C. Spiel, Y. Suchorski, A. Trincherro, R. Schlogl, H. Gronbeck and G. Rupprechter, *Angew. Chem., Int. Ed.*, 2012, **51**, 10041–10044.
- 152 M. Rycenga, J. M. McLellan and Y. Xia, *Adv. Mater.*, 2008, **20**, 2416–2420.